Identifying the Flow Conditions in Pneumatic Conveying of Wheat Grains through Horizontal Straight and Bent Pipe using Pressure Drop

A Thesis Submitted to the College of

Graduate Studies and Research

In Partial Fulfillment of the Requirements

For the Degree of Master of Science

In the Department of Mechanical Engineering

University of Saskatchewan

Saskatoon

By

Lav Mittal

Permission to Use

In presenting this thesis in partial fulfillment of the requirements for a Postgraduate degree from the University of Saskatchewan, I agree that the Libraries of this University may make it freely available for inspection. I further agree that permission for copying of this thesis in any manner, in whole or in part, for scholarly purposes may be granted by the professors who supervised my thesis work or, in their absence, by the Head of the Department or the Dean of the College in which my thesis work was done. It is understood that any copying or publication or use of this thesis or parts thereof for financial gain shall not be allowed without my written permission. It is also understood that due recognition shall be given to me and to the University of Saskatchewan in any scholarly use which may be made of any material in my thesis.

Requests for permission to copy or to make other uses of materials in this thesis in whole or part should be addressed to:

Head of the Department of Mechanical Engineering

University of Saskatchewan

57 Campus Drive

Saskatoon, Saskatchewan, S7N 5A9, Canada

OR

Dean

College of Graduate Studies and Research

University of Saskatchewan

107 Administration Place

Saskatoon, Saskatchewan, S7N 5A2, Canada

Abstract

Pneumatic conveying is a process of transporting solids, such as granules, powder, and other bulk materials, in a gas stream through pipelines. One among many of its applications is seen in agricultural air seeders, which are used for seed planting and applying granular fertilizers. One of the most reported problems in a pneumatic conveying operation is blockage (partial/complete) of the pipeline, which occurs due to the prolonged settling of conveyed material in the pipeline. When the material settling or pipe blockage occurs during the conveying process, the overall efficiency drops significantly.

Various kinds of sensors are popularly used in the pipelines to detect the settling or blockage during the conveying operation. However, these available sensors are not able to detect the onset conditions beyond which settling or blockage generally occurs. Therefore, these sensors do not enable pro-active actions to be taken.

Some previous research has illustrated that the trend of the pressure drop in a pipeline during a pneumatic conveying process represented the corresponding flow conditions. Moreover, the trend showed a transition when the flow conditions became close to the settling conditions. These characteristics suggest that the pressure drop in a pipeline could be used to detect the approaching adverse flow condition (settling condition) before the actual settling occurs, and thus can help in identifying the optimal operating point. In addition, some studies have observed that the trend of pressure drop per unit length of pipe (pressure gradient) for a given set of flow conditions might differ with different kinds of solid materials, pipe configurations, and operating conditions.

Only a few studies have presented experimental data for the pneumatic conveying of wheat grains. This thesis research was aimed at extending the understanding of the applicability of the pressure drop in identifying the corresponding flow conditions and the optimum air flow rate for the pneumatic conveying of the wheat grains. This project also filled some gaps in the literature by conducting the experiments in a 57 mm ID horizontal pipeline for three different grain feed rates (20 - 100 g/s) and ~17 different air flow rates. To understand the effect on the pressure drop and the flow conditions upon bending the pipeline, the experiments were conducted with horizontal-straight as well as horizontal-bent pipe (with four different angles: 22.5°, 45.0°, 67.5°, and 90.0°).

The results showed that the trend of pressure drop over a range of air speeds could successfully identify the occurrence of the grains settling. The air speed corresponding to the minimum pressure drop consistently appeared to be slightly higher than the air speed at which the grains started to settle in the pipe. Therefore, the air speed corresponding to the minimum pressure drop can be recommended as the threshold and optimum air speed. The effect of bending the pipe on the pressure drop and the settling speed were found to be just minimal, probably because of the fan controller system (which maintained the air speed constant during the test) and the large radius of bend. Also, by measuring the pressure drop in local sections of the pipeline, the locations of major settling could also be successfully identified.

Acknowledgements

I express my deepest gratitude to my supervisors, Dr. Scott D. Noble and Dr. David Sumner, for accepting me as a graduate student, and for their constant guidance and support during my M.Sc. program. I am also very grateful for their generosity and kindness which always inspire me.

I am very much thankful to Dr. Noble for his great efforts and time in explaining the technical concepts, making me learn new things, discussing the research, and guiding me on the thesis writing. I highly appreciate his warm attitude, advice, patience, and humility in all conditions. Words are not enough to thank Dr. Noble for his efforts, kindness, and words of encouragement when I needed them most.

My sincere thanks to Dr. Sumner for his great help and guidance in research and thesis writing. I cannot thank him enough for the moral support and encouragement he provided at every step and in all circumstances. I greatly appreciate that he was always there to answer all my questions, and to suggest the best but the simplest way to do things. I am deeply thankful to Dr. Sumner for his patience, time, and great help in completing my thesis.

I express my heartiest thanks to Dr. David A. Torvi for his guidance in my application process for the M.Sc. program. I also thank my advisory committee members: Dr. Donald J. Bergstrom and Dr. James D. Bugg, for their input and suggestions on my research work. I acknowledge the kind help I received from the staff members of the department of Mechanical Engineering.

Warm thanks to Mr. Tyrone Keep for his time and efforts in explaining things in the lab and in helping me out in the mechanical workshop. It was great to share an office with him and to

have interesting discussions. I am also thankful to Mr. Shabbir Hossain for his help in preparing the lab and sharing his experiences. It was also great to have friends like Mr. Ayodele Ogunremi and Mr. Houman Kamali.

Heartiest thanks to my family: parents, uncle, aunt, brother, sister-in-law, and sisters for their unconditional love, sacrifices and for being my strength and support in every moment. A special thanks to my brother, Mr. Kushagra Mittal, for being my mentor, an unconditional support, and a protective shell. It was impossible to complete my thesis and M.Sc. program without his immeasurable help and support. I also thank my sister-in-law, Ms. Aditi Saini, for sharing her research experience, guiding me in various things, and being very supportive. Also, it was the constant motivation, guidance, and support from Mr. Mittal and Ms. Saini, which made it possible for me to have an opportunity to study at prestigious University of Saskatchewan.

My sincere thanks to Mr. Jim Henry, Mr. Joel Gervais, and CNH Saskatoon for the funding, equipment, and support provided for this research project. The Natural Sciences and Engineering Research Council of Canada is also gratefully acknowledged. Last but not the least, I thank every one who helped me directly or indirectly in my M.Sc. program.

Table of Contents

List of Tables

List of Figures

Nomenclature

Greek Symbols

ε	Venturi expansion factor
θ	Pipe layout or pipe bend angle
K	Von Karman constant
λ	Friction factor of pipe
μ	Dynamic viscosity of gas
ρ	Air density
ρ_g	Gas density

English Symbols

A	Cross sectional area of conveying line
A_p	Projected area of particle normal to the gas flow
B	Barometric pressure
C	Venturi calibration constant
C_D	Drag coefficient
C_{VD}	Venturi discharge coefficient
D	Diameter of conveying line
D_1	Diameter of venturi upstream
D_2	Diameter of venturi throat
D_p	Pipe diameter
dp	Equivalent spherical diameter of pipe
D-1	Data acquisition unit (DAQ) used in air flow rate measurement
D-2	Data acquisition unit (DAQ) used in pressure data measurement

$f(P,T)$	Enhancement factor for saturation vapor pressure
L	Pipe length
Ma	Molecular mass of dry air
$\dot{m}_p$	Grain feed rate
M_v	Molecular mass of water vapor
p_o	Absolute pressure at venturi upstream
P_{throat}	Pressure transmitter measuring the differential pressure between venturi upstream and throat
p_{static}	Static pressure measured by Pitot-static probe
p_{sv}	Saturated vapor pressure
$P_{upstream}$	Pressure transmitter measuring the absolute pressure at venturi upstream
$p_{velocity}$	Velocity pressure measured by Pitot-static probe
ΔP	Pressure gradient or pressure drop per unit length of pipe
ΔP_{avg}	Average pressure gradient in the entire length of pipe
ΔP_L	Pressure drop in L length of pipe
ΔP_{local}	Local pressure gradient in a local section of pipe
$\Delta P_{local\text{-}bend}$	Local pressure gradient in bend section of pipe
$\Delta P_{local\text{-}downstream}$	Local pressure gradient in section downstream of bend
$\Delta P_{local\text{-}L_1}$	Local pressure gradient in L_1 section of pipe
$\Delta P_{local\text{-}L_2}$	Local pressure gradient in L_2 section of pipe
$\Delta P_{normalized\text{-}local}$	Pressure gradient with grain flow normalized by the corresponding pressure gradient in air only flow
$\Delta p_{venturi}$	Differential pressure between upstream and throat of the venturi
Q_m	Air flow rate measured by venturi

R	Specific gas constant
Re_p	Particle Reynolds number
RH	Relative humidity of air inside the venturi
T_0	Room air temperature
T_v	Temperature inside the venturi
u_{cr}	Critical speed
u_g	Air speed measured by venturi
u_{gas}	Gas speed
u_r	Relative velocity between gas and particle
u_{set}	Settling speed
v	Air speed measured by Pitot-static probe
z_v	Air compressibility factor

Chapter 1 : Introduction

Material transport has always been of great interest to humankind. Transportation of fluids through pipelines is a common practice in industrial as well as domestic applications, whereas, solid material transportation through pipelines is becoming popular in various industrial sectors. For transporting the solid material through a pipeline, a pressurized fluid is generally required as a carrier medium for carrying the solid material from one place to another. When solid materials such as granules, powder, and other bulk materials are transported in a gas stream, the process is known as pneumatic conveying (Cabrejos & Klinzing, 1995). Because the air is available in abundance and free of cost, it is the most common gas used in pneumatic conveying processes. However, in conditions when the solid material can react with the air and may cause fire, health, or explosion hazards, other alternative gases (carbon dioxide, nitrogen, etc.) are preferred instead of air (Klinzing et al., 2010).

Pneumatic conveying systems are classified in to two categories: positive pressure and negative pressure (vacuum) systems. Positive pressure conveying systems are generally preferred for conveying the material from a single feeding point to one or several destinations. Negative pressure conveying systems are usually preferred for transporting the material from multiple feeding points to one or several destinations (Klinzing, et al., 2010). In the present thesis research, a positive pressure system has been used for conveying wheat grains from a tank to a receiving bin through a 11.6 m long horizontal pipeline. The sketch in Figure 1.1 shows the concept of positive pressure pneumatic conveying through a horizontal pipe.

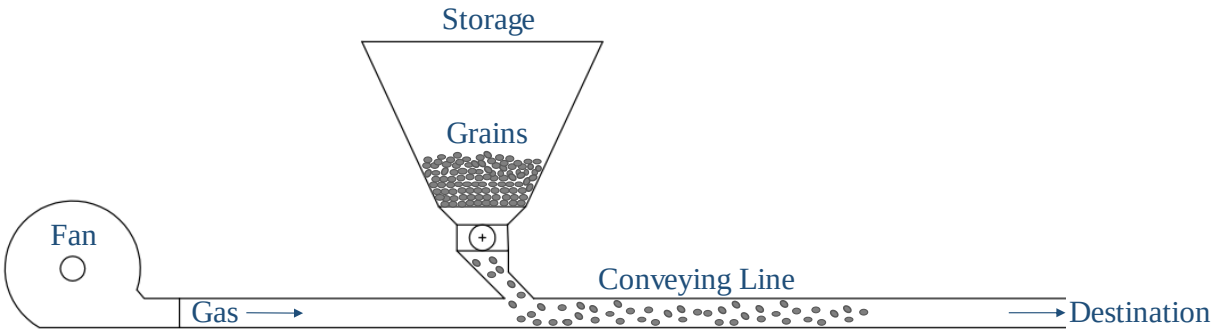

Figure 1.1: Illustration of the concept of positive pressure pneumatic conveying in a horizontal plane.

Pneumatic conveying has many attractive features such as flexible routing, secured transportation, and minimal maintenance (Klinzing, et al., 2010), which make it a popular method of solid material transportation in various industries such as coal, cement, polymer, and pharmaceuticals. Besides the industrial applications, pneumatic conveying has also revolutionized the agricultural practices by its application in agricultural machines (air seeders) for seed planting and for applying fertilizers. Today, a majority of farmers in the Northern Great Plains use air seeders for seeeding.

In a pneumatic conveying process, a fundamental objective is that the conveyed material reaches its target destination at the same rate at which it was introduced into the conveying line and with its properties intact. This essentially requires a stable and continuous flow inside the conveying line throughout the process, which often gets disturbed when the conveyed material starts to settle down on the bottom of pipe before reaching the destination. This condition of material settling results in a loss of productivity for a continuous conveying process as the rate of delivery becomes lower than the rate at which the material was introduced in the conveying line. For example, the settling of seeds or fertilizers in the conveying lines of an air seeder causes less seeds and fertilizer being planted/spread over the farming land. Moreover, if the settling in the

conveying line continues, the settled layers of material may completely block the conveying line. Blockages result in downtime and additional maintenance cost of the conveying system. Thus, to maintain the stability of the conveying process, it seems highly important to identify the settling of grains as soon as it happens, or even before it occurs.

Although maintaining a high air speed might seem to be an easy solution to completely avoid the risk of settling, such a process would require excessive amounts of energy, and may also cause damage to the particles and pipe wall due to intense collisions. Therefore, pneumatic conveying systems must be operated at an appropriate gas flow rate such that the settling and blockage do not occur, and that damage to the material and pipe are maintained to an acceptable level. However, in practical situations even upon starting the conveying process with a gas flow rate above the threshold (minimum conveying air speed), the blockage of conveying lines due to settling is commonly observed during the process. Therefore, it is highly important to continuously monitor the flow condition during the conveying process and take corrective action when there is a risk of adverse flow conditions (settling or blockage).

Different kinds of sensor-based systems are employed in pneumatic conveying systems to detect and control the condition of settling or blockage. Some of the commonly used sensors are acoustic (Albion, et al., 2007), LED (Tevs, et al., 2003), and piezoelectric (Thomas, et al., 1998). The available monitoring systems function by detecting the settling or blockage in the conveying line, however they do not claim to detect the conditions that precede settling, so that the settling can be avoided rather than cleared after it occurs. Some previous research has indicated that the pressure drop in the conveying line during the operation can represent the corresponding flow conditions. Moreover, when the flow condition arrives close to the settling condition, the trend shows a detectable transition. In addition to that, some studies have observed that the trend of

pressure gradient for the corresponding flow conditions might be more or less different with different kinds of solid materials, pipe configurations, and operating conditions.

This thesis research project was aimed at extending the understanding of the applicability of the pressure drop to identify the flow conditions in pneumatic conveying of wheat grains. The experiments were conducted for a wide range of operating conditions and the trend data (pressure drop) were analyzed in different ways. The objectives, methodology, and research contributions of this study are presented in the following subsections.

1.1 Objectives

The objectives of this thesis project were to investigate:

- the effect of pipe layout (straight and bent) on the flow characteristics and grain settling pattern;
- the pressure drop trend in different layouts (straight and bent) of horizontal pipe, its utility in identifying the corresponding flow conditions, and its feasibility to suggest an optimum air speed for which the energy consumption is minimum and the flow continues without grain settling;
- the difference between the local pressure drop trend in different sections of pipe (upstream of bend, bend, and downstream of bend), and to analyze which of them would be the most consistent and informative; and
- the utility of the pressure drop in identifying the location of settling in a non-transparent pipe.

1.2 Methodology

The experimental data were collected by conducting the tests of pneumatic conveying of wheat grains in a 57 mm ID horizontal pipeline for three different grain feed rates (20, 60, and 100 g/s) and ~17 different air flow rates. To understand the effect on the pressure drop and the flow conditions around a bend in the pipeline, the experiments were conducted with horizontal straight

as well as horizontal bent tubing at four different bend angles (22.5°, 45.0°, 67.5°, and 90.0°). The data were analyzed in different ways to explore their possible utilization in flow identification.

1.3 Research contribution

Only a few studies have previously presented the experimental data for the pneumatic conveying of wheat grains. This study attempted to fill some gaps in the literature by collecting the experimental data for a wide range of operating conditions and by presenting the results from the data analysis. This study showed that the pressure drop trend could successfully represent the corresponding flow condition, and also effectively indicated when (in terms of air speed) and where the grains settled down in the pipe. This study also provided the results which were different from some of the pre-experiment assumptions, and the data analysis provided its explanation. The experiments illustrated that the use of a fan controller system (for maintaining a constant air speed irrespective of the flow condition) was very useful in overcoming the additional effect of the bend on the flow. The results indicated that by using a fan controller system (for maintaining a constant air flow rate in all conditions), the chances of grains settling and pipe blockage can be minimized.

1.4 Thesis overview

The background and the literature review related to the pressure measurement and its utility in horizontal pneumatic conveying are presented in Chapter 2. Chapter 3 presents a description of the experimental setup and the measurement methodologies. Chapter 4 presents detailed discussion of the experimental methods, observations, data, and results outlining the applicability of pressure measurement in pneumatic conveying processes. The conclusions and future work are summarized in Chapter 5. Appendix A presents the equations used for air density measurement, and Appendix B presents all the additional data plots which were not shown in Chapter 4.

Chapter 2 : Literature Review

2.1 Flow condition in pneumatic conveying

The flow conditions in a pneumatic conveying process depend on different factors such as properties of the solid and gas phases, solid feed rate, gas flow rate, and pipe geometry (Mills 2004, Dhole et al. 2011). The characteristics of particle suspension in a gas stream also depend on the particle size and density difference between the solid and the gas (Geldart, 1973). One of the most dominant factors is the ratio of solid feed rate and gas flow rate, known as the loading ratio (Mills 2004, Klinzing et al. 2010). Conveying processes with loading ratios ≤ 15 are classified as dilute flow; whereas processes with higher loading ratios are characterized as dense flow. Alternatively, some studies defined the flow conditions transition in terms of volumetric concentration, such as Konrad (1986), which suggested that the flows with greater than 10% (v/v) tend to fall in the dense flow regime, whereas another study, Santos, et al. (2011), suggested this transition to occur at 1% (v/v).

The solid particles in a dilute flow are well suspended in the gas flow, whereas the particles in a dense conveying regime can flow in several forms such as dunes, layers, plugs, etc. (Cabrejos & Klinzing 1995, Suji & Morikawa 1982, Herbreteau & Bouard 2000, Jama et al. 2000, Barbosa & Seleghim Jr. 2003, Molerus & Burschka 1995, Fraige & Langston 2006, Rabinovich & Kalman 2011). Both of these flow types have their own advantages and disadvantages. Dense flow conveying is suitable for the applications where the time and the gas flow rate efficiencies are of special interest (Konrad, 1986). On the other hand, dilute flow is considered more suitable for the applications where the continuous and uninterrupted flow of the particles is of utmost importance (Hapman, 2005).

During a pneumatic conveying process, the solid particles can be completely, partially, or not at all suspended in the gas stream depending on their properties and operating conditions. However, in general terms, the probability of the particle suspension increases with increasing gas flow rate due to greater lift force and high turbulence (which helps in faster momentum transfer). Similarly, upon decreasing the gas flow rate, the suspension reduces and the concentration of particles moves towards the bottom of pipe due to decreased lift force and lesser turbulence. Furthermore, if the gas flow rate is below a minimum threshold, the particles can not be suspended in the gas and are observed to slide and roll and then settle down in the form of layers on the bottom of the pipe. A prolonged settling may also turn in to the blockage of the pipe which is strictly undesired in all types of pneumatic conveying applications. Therefore, the information about the threshold gas flow rate at which the particle settling begins to occur is crucial in a pneumatic conveying process (Albion et al. 2007, Gomes & Mesquita 2014).

2.2 Particle motion in pneumatic conveying

The flow condition in a horizontal pneumatic conveying process is characterized by the condition of particles' suspension in the gas stream. The turbulence of gas stream is a contributing factor in particle suspension, however, the more dominating factor in it is the Magnus effect. In a horizontal gas-solid pipe flow, the particle acquires a spin from the gas turbulence, the torque caused by the gas velocity gradient (across the pipe diameter), and its collisions with the pipe wall. Because of the spinning motion of particle, a pressure gradient is developed across its surface, which results a lift force causing the particle motion in transverse direction. This effect is known as the Magnus effect. The direction of lift force depends on the direction of particle rotation and the relative velocity between the gas and the particle.

In a pneumatic conveying process, since the gas flow is turbulent and multiple particles are introduced at a time, both the direction of particles' rotation and the resulting direction of lift force are random and dynamic. Therefore, the lift force on particles in pneumatic conveying act in several transverse directions along the flow path. For large particles (diameter > 1mm), the Magnus effect plays a significant role in particles' suspension (transverse motion), however, the major contributing factor for suspension in that case is the irregular bounces of particles due to their collisions with the pipe wall (Matsumoto & Saito, 1970). The effect of these bounces become even more significant for non-spherical particles (having irregular shape and surface) and rough pipe wall.

As the gas velocity increases in the pneumatic conveying process, the particles' spinning rates increase and the resulting lift force (Magnus effect) also increases. For high gas velocities, the particles collide more intensely with the pipe wall and thus provide more irregular bounces across the pipe diameter. Therefore, the particles are more uniformly dispersed at high gas velocities. Whereas, with reduction in gas velocity, the lift force as well the bouncing effect are reduced due to the slower spins of particles and their less intense collisions with pipe wall. Therefore, the particles' dispersion becomes less uniform. That is why in a horizontal pneumatic conveying process, the particles' concentration becomes higher in the lower half of pipe at low gas velocities, as the gravitational force starts dominating over the lift forces. Moreover, when the gas velocity reaches below a minimum threshold, the lift force (caused by the Magnus effect) as well as the effect of irregular bounces of particles are too weak to result the transverse motion of particles across the pipe diameter. In this condition, the gravitational force dominate over the lift force and the particles start settling down in the pipe bottom.

A particle's motion in the axial direction largely depends on the drag force (F_D) acting on the interface of gas and particle. The expression for the drag force by the gas on a particle is given in Equation 2.1. The direction of the drag force depends on the relative velocity between the gas and the particle, and a part of the drag force may also contribute in the transverse motion of the particle.

$$F_D = C_D \rho A_p u_r^2 \qquad \textbf{Equation 2.1}$$

where,

F_D = Drag force,
C_D = Drag coefficient,
ρ = Gas density,
A_p = Projected area of particle normal to the gas flow, and
u_r = Relative velocity between gas and particle.

The drag coefficient (C_D) is a function of particle Reynolds number (Re_p), and in pipe flow is calculated by using Equation 2.2 (Gupta & Pagalthivarthi, 2006):

$$C_D = 0.44 \quad \text{when } Re_p > 1000$$

$$C_D = (24 / Re_p)(1 + 0.14\, Re_p^{0.7}) \quad \text{when } Re_p \leq 1000 \qquad \textbf{Equation 2.2}$$

and,

$$Re_p = \frac{\rho\, u_r\, d_p}{\mu} \qquad \textbf{Equation 2.3}$$

where,

d_p = Equivalent spherical diameter of particle, and

μ = Dynamic viscosity.

A schematic diagram in Figure 2.1 shows the free-body diagram of a particle in two different stages of flow in pneumatic conveying.

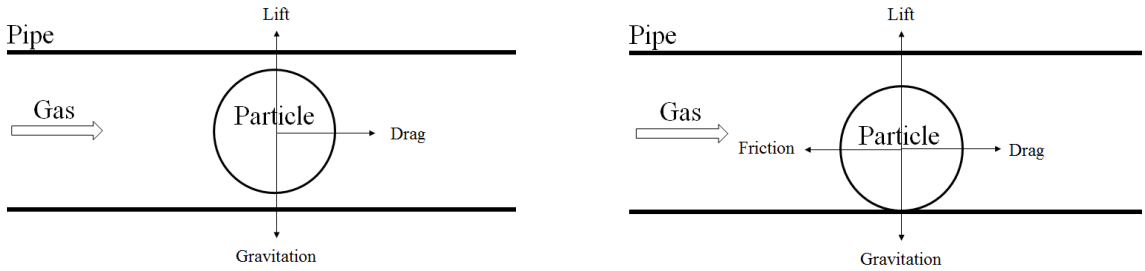

(a) Particle suspended in gas (b) Particle settled in pipe bottom

Figure 2.1: Free-body diagrams of a particle in horizontal pneumatic conveying.

At a low gas velocity (below the minimum threshold), when the gravitational force dominates over the lift force, the particle falls from the suspension and crawls/rolls on the pipe bottom. In this condition, the friction between the particle and the pipe wall opposes the drag force on the particle. When the gas velocity is such low that the drag force (which depends on relative velocity u_r) is not enough to overcome the friction between the particle and the pipe wall, the particle stops moving axially and settles down permanently. In case of multiple particles flow in gas, the friction between the particle-particle also contributes in the resistance against the drag force.

2.3 Pressure drop in pneumatic conveying

In a gas flow through a pipe, the pressure drop occurs because of the resistance to the gas flow caused by the friction between gas and pipe wall. This pressure drop can be calculated from the Darcy-Weisbach expression (Equation 2.4).

$$\Delta P = \frac{\lambda \rho L u_g^2}{2D_p}$$ **Equation 2.4**

where,

ΔP = Pressure drop in L length of pipe,

λ = Friction factor,

ρ = Gas density,

L = Pipe length,

u_g = Gas speed, and

D_p = Pipe diameter.

In a two-phase (gas-solid) flow, the pressure drops not only because of the friction between the pipe wall and the gas, but also the drag force offered by the particles. Because the drag is directly proportional to the relative velocity (u_r) between gas and particles, the drag force acting on the gas is fairly high when the particles' velocity is much lower compared the gas velocity. That is why the local pressure drop in the particles entrainment zone is high as the particle have very low axial velocity when introduced in the gas stream, and start accelerating thereafter. At high gas velocities, the particles are dispersed and are accelerated up to 70 % - 90% of the gas velocity. Therefore, small relative velocity between gas and particles causes small drag force on the gas. At high gas velocities, the major part of the pressure drop is due to friction losses. At low gas flow rates, when the particles are not dispersed in the gas and are moving slowly in the form of groups and layers in the pipe bottom, the drag force on the gas flow is very high, causing a significant pressure drop. Similarly, the pressure drop is even much higher when the particles settle down and form stationary layer in the pipe bottom.

The gas-solid flow through the bend in a pipe is more complex than in a straight pipe. In a bend, the gas flow acquires a double vortex structure, and because of the centrifugal force, the

particles get separated from the gas (Rinoshika, 2014). Being heavier, the particles concentrate along the outer radius of the bend (Dhodapkar et al. 2009, Michaelids & Lai 1987, Rinoshika 2014). The higher concentration of particles along the outer radius, which appears as a "rope" of particles, causes the extended contact and collisions among the particles and the pipe wall. This results in a significant drop in particles' velocity in the direction of gas flow. The rope structure of particles (separated particles from the gas) lasts into the downstream section of the bend and then the particles again get reaccelerated and entrained in the gas stream by the virtue of gas turbulence and double vortex flow caused by the bend (Rinoshika, 2014). The double vortex flow of gas occurs in bend and downstream because of the deformed axial velocity profile of the gas caused by the cross-stream pressure gradient in those regions (Rinoshika, 2014). The energy being consumed in reacceleration of the particles in the downstream of bend causes the additional pressure drop. Thus the bend effect on the pressure drop includes the deceleration of particles along the bend due to the excessive friction and the reacceleration of particles for their re-entrainment in the gas flow (Dhodapkar et al. 2009). The bend effect depends on the bend radius. The smaller the radius, the more the bend would affect the particles' flow in terms of particle separation, collisions, deceleration, and reacceleration. Also, the higher the bend angle (for a given radius), the longer the bend length would be. Other factors such as gas flow rate, solid feed rate, void fraction may also play a vital role in determining the bend effect.

In the literature there are several studies which were conducted to determine the bend effect, however, because of the limited operating conditions tested, multiple variables, and limited data disclosed, any particular finding cannot be generalized. Therefore, this study attempted to collect the data to analyze the bend effect for the target operating conditions (bend radius, bend angle, solid feed rate, air flow rate).

2.4 Existing means to detect the settling

Researchers and engineers have proposed a number of techniques to detect the particle settling conditions and pipe blockage during the pneumatic conveying operation. These techniques basically use sensors to monitor the particle flow rate and to detect when the fewer particles pass by the sensor due to the particle settling upstream. Some of these sensors include, but are not limited to acoustic (Albion et al. 2007, Gelinske et al. 2015), optical (Tevs et al., 2003), and piezoelectric (Thomas et al., 1998). An optical sensor operates on the principle of differences in light absorbance and reflectance of the solid particles based on their concentration in any given plane (Tevs et al., 2003). The sensor is mainly comprised of a light source (e.g., LED) that emits a constant intensity light beam from one side of the pipe, and a receiver (e.g., phototransistor) that detects the change in the intensity of the light beam due to the passing by of the particles. When the receiver detects the intensity beyond the allowable limit, it generates an alarm as a sign of the particles settling upstream. Similarly, the piezoelectric and the acoustic sensors measure the particles' flow condition on the basis of analog and sound signal, respectively. Although the aforementioned sensors effectively detect the condition of particle settling or blockage in pipe, they do not provide any warning of the approaching adverse flow condition before the particles actually start settling. Thus, the application of these sensors is limited to notify the operator/controller so that the corrective measures can be taken, but not to avoid the occurrence of settling/blockage in the first place.

Barbosa, et al. (2010) demonstrated that self-organizing neural networks (a special class of artificial neural networks) could identify the flow regime in a horizontal pneumatic conveying process very effectively. The neural network system is complex in nature as it is a large network of interconnected processing units which require training data and training procedure to function,

which make it a complex method to be developed and implemented. On the other hand, some researchers (Zenz 1949, Thomas 1962, Konrad 1986) have illustrated that the pressure drop in a pipe during a pneumatic conveying process could effectively indicate the corresponding flow conditions. Also, because the pressure drop in the conveying line during a pneumatic conveying process is directly related to the flow condition inside the pipe, it perhaps provides the closest link to the corresponding flow characteristics.

In one of the very first such studies, Zenz (1949) investigated the effect of the flow conditions on the pressure drop during the pneumatic conveying of four different types of particles, namely rapeseed, glass beads, sand, and salt. The pressure drop data were recorded for three solid feed rates and for a range of air speeds in straight horizontal and vertical pipes, and the flow conditions inside the pipe were visually observed. The generic form of the curves obtained by Zenz from the horizontal pneumatic conveying experiments are presented in Figure 2.2.

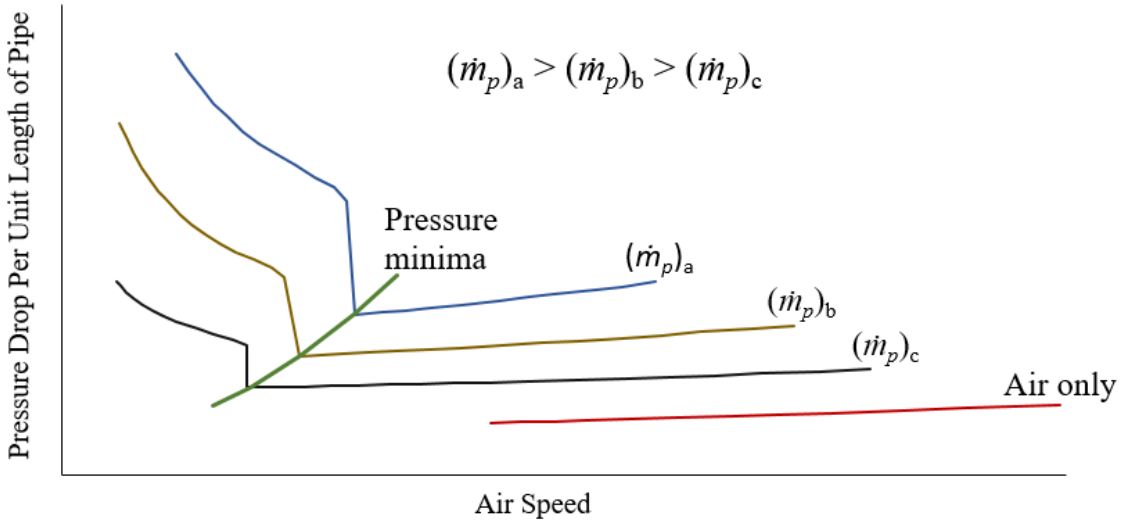

Figure 2.2: Generic form of the pressure trend curves obtained by Zenz (1949). $(\dot{m}_p)_a$, $(\dot{m}_p)_b$, and $(\dot{m}_p)_c$ represent three different solid feed rates: $(\dot{m}_p)_a > (\dot{m}_p)_b > (\dot{m}_p)_c$.

Zenz (1949) observed that at any given air speed the average pressure drop in presence of solid particles was always higher than the corresponding pressure drop for air only flow. For air only flow, the pressure drop decreased monotonically upon lowering the air speed, however, the trend changed significantly upon introductions of solid particles in the flow. For example, when the solid particles were fully suspended in the flow (dilute flow at relatively higher air speed), any reduction in the air speed resulted in smaller pressure drops, similar to the air only flow. However, the trend reversed upon reaching a minimum pressure drop, beyond which pressure started to increase with any further reduction in the air speed. Zenz (1949) also noted that the air speed corresponding to the minimum pressure drop (hereafter referred to as *critical speed*) was the very same point where the flow transitioned from dilute to dense. The overall shape or qualitative trend of the pressure drop curves in Zenz's study remained unchanged irrespective of the solids feed rate, however the curves shifted upward-right with increasing solid feed rate (i.e. higher pressure drops and higher critical speed). Zenz (1949) also observed that all four tested solid materials started settling when the air speed reached just below the critical speed. Upon further reduction in air speed a larger number of grains settled down and the thickness of the settled layers increased. Similarly, some other studies (Santos et al. 2011, Kai et al. 2013) also obtained the settling speed below the critical speed.

On the contrary, a few studies (Cabrejos & Klinzing 1995, Hong et al. 1995, Akilli et al. 2005) suggested that the saltation speed (at which the particle dropped from the suspension and slid on the bottom of pipe) and the settling speed (at which the particles formed a stationary layer on the bottom of pipe) were not always lower than the critical speed (corresponding to minimum pressure drop), and largely depended on the particle shape and size. Specifically, (Cabrejos & Klinzing 1995 and Hong et al. 1995) found the saltation (particles dropped from the suspension)

of coarse materials to occur exactly at the critical speed, whereas, for the flake-like alumina material, the settling was found to occur at an air speed higher than the critical speed (i.e. it was at the right side of the minimum pressure drop point). Along with this, two patents (Goering et al. 2007, Smith 2008) disclosed the use of pressure measurement in detecting the blockage condition in combine harvesters, however the disclosed methodologies were largely dependent on the specific design of the harvester and the location of the pressure sensors. The aforementioned studies highlighted the significant effect of the particle properties (density, shape, and size) on the pressure drop trend and the settling speed, and indicated that using the pressure drop trend to identify the flow condition depends upon pressure data being collected from the same conveying system and particles.

2.5 Focus of thesis research

The focus of this thesis project is to explore the applicability of pressure drop data in identifying the flow condition in horizontal pneumatic conveying of wheat grains so that the settling could be avoided or at least could be detected in a timely fashion. There were many studies in the literature which collected pressure drop data in pneumatic conveying tests, however, there seems to be a dearth of experimental data in the literature for pneumatic conveying of wheat like particles. Guner (2007) conducted the tests for pneumatic conveying of wheat grains and three other types of seeds (barley, lentil, and sunflower), however the air speed in the tests were not lowered to the extent where the settling condition could have appeared. Moreover, the observation that the highest pressure drop occurred for the wheat grains among all tested materials highlighted the uncommon flow characteristics of the wheat grains.

To fill the apparent gap in the literature and to extend the understanding of the flow patterns as well as settling pattern in pneumatic conveying of wheat grains (non-spherical with an aspect

ratio of 2.3:1), tests were conducted in the present thesis research to collect and analyze the pressure drop data along a horizontal pipe for a range of grain feed rates (20-100 g/s) and pipe layouts (0°-90° bend angle). The data analysis aimed to examine the feasibility of pressure drop in identifying the flow condition in the pneumatic conveying of wheat grains through different pipe layouts (straight and bent). It was expected that the knowledge from this study would not only be helpful in understanding the applicability of the pressure drop data for pneumatic conveying of wheat grains but also to visualize the effect of solid feed rates and pipe layout (bend angle) on the settling characteristics. The testing with the wheat grains is very important because it is one of the most popular and valuable crop in North America, and its plantation is done by using the pneumatic conveying system of an air seeder. This study is expected to assist in improving the design and operations of the air seeders which are widely used in North America.

Chapter 3 : Experimental Setup

This chapter provides a description of the experimental setup which was built and installed in the Air Handling Lab, College of Engineering, at the University of Saskatchewan. A schematic diagram of the setup is provided in Figure 3.1. The experimental setup includes four main units: the air supply system, the solid material (wheat) storage and metering system, the conveying line (pipe), and the data acquisition unit.

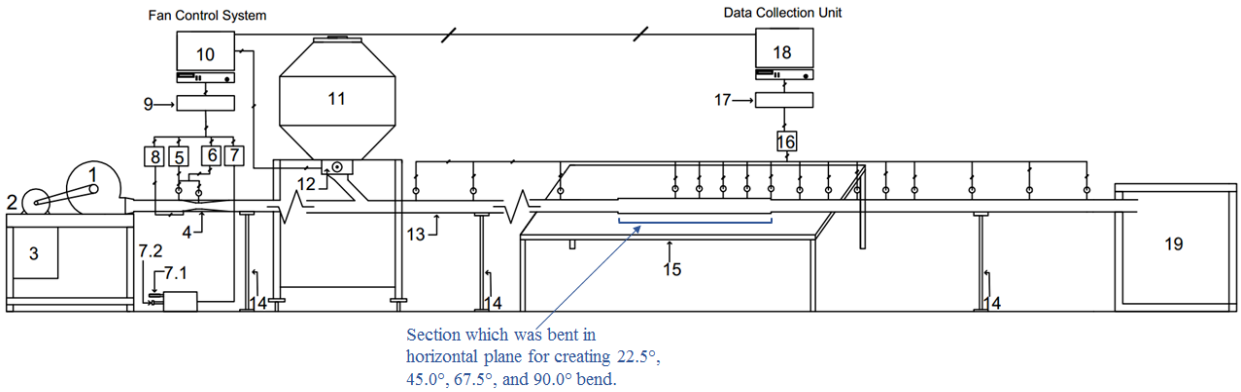

Figure 3.1: Schematic diagram of the experimental setup. The numbered components are listed in Table 3.1.

Table 3.1: List of the components of the experimental setup.

Number	Component	Number	Component
1	Centrifugal fan	10	Computer-1 (for fan control system)
2	Electric motor	11	Wheat grains storage tank
3	Variable frequency drive (VFD)	12	Metering system (feed roller and stepper motor)
4	Venturi meter	13	Conveying line (pipe)
5	Gauge pressure upstream of venturi	14	Supporting stand
6	Differential pressure between venturi upstream and venturi throat	15	Supporting bed
7	Signals from weather station (room temperature, pressure, and humidity)	16	Differential pressure in 15 different sections along the conveying line
7.1	Room temperature and humidity sensor	17	DAQ (*D-2*) in data collection unit
7.2	Room pressure sensor	18	Computer-2 (for data collection unit)
8	Air temperature inside the venturi	19	Grains collection bin
9	DAQ (*D-1*) in fan control system		

3.1 Air supply system

The main purpose of the air supply system was to deliver, measure, and control the air flow in the conveying line. The system was made of three main segments: (i) the fan assembly (ii) the venturi meter, and (iii) the fan control system.

3.1.1 Fan unit

A centrifugal fan, powered by an electric motor, was used to provide the air supply during the experiments. The speed of the motor was controlled by a variable frequency drive (VFD). The fan unit is shown in Figure 3.2, and the specifications of the aforementioned components are presented in Table 3.2.

Figure 3.2: Fan unit in the air supply system showing centrifugal fan, motor, and VFD components.

Table 3.2: Specifications of the components in the fan unit.

Component	Specifications	Make/Supplier	Model
Centrifugal fan	Similar to one used in Flexi-Coil air cart	Flexi-Coil	
Electric motor	3.7 kW (5.0 HP), 60 Hz, 230 V, Three-phase	Marathon Electric	JVB184TTFW 6001AA M
VFD	3.7 kW (5.0 HP), 230 V, Three-phase	AutomationDirect	GS2-25PO

3.1.2 Venturi meter

A venturi meter, having the specifications very close to ISO standard (ISO 5167-4, 2003), was used for measuring the air flow rate (schematic provided in Figure 3.3). The venturi was calibrated against a Pitot-static probe. The internal diameter (ID) of the upstream (D_1) and the throat (D_2) sections of the venturi were 91.7 mm and 45.8 mm, respectively. The venturi was fitted inside a steel pipe of ID 102.8 mm, and was installed downstream of the fan's outlet as shown in Figure 3.4.

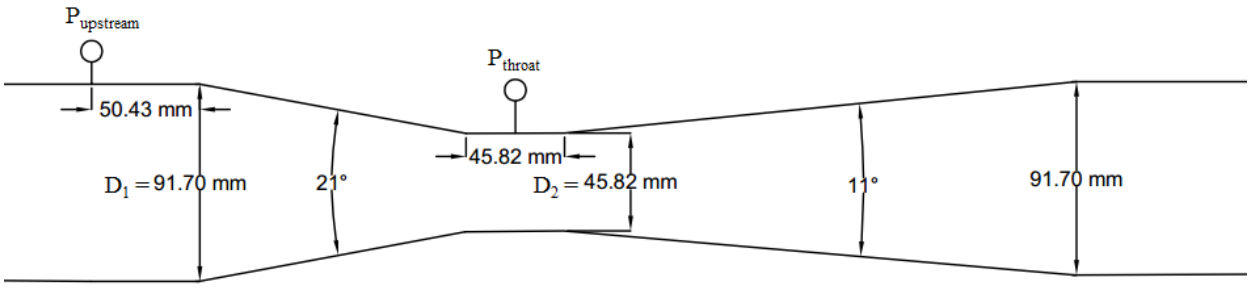

Figure 3.3: Schematic diagram of venturi meter, built according to ISO 5167-4:2003, used for air flow rate measurement in this study. $P_{ustream}$ and P_{throat} are the pressure transmitters measuring the absolute pressure at venturi upstream and differential pressure between venturi upstream and throat, respectively.

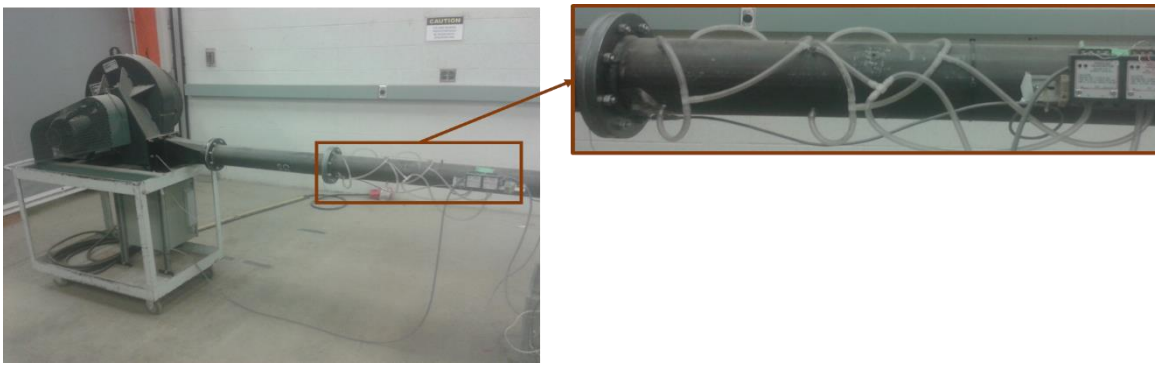

Figure 3.4: External view of the venturi meter installed at downstream of the fan's outlet.

3.1.2.1 Air flow rate measurement

The air flow rate (Q_m) was measured by Equation 3.1 which is according to the ISO 5167-4, 2013 standard:

$$Q_m = C_{VD}\ \varepsilon\ \frac{1}{4}\ \pi\ D_2^{\,2}\ \frac{1}{\sqrt{1-\left(\frac{D_1}{D_2}\right)^4}}\ \sqrt{2\ \Delta p_{venturi}\ \rho},$$

Equation 3.1

where,

C_{VD} = Venturi discharge coefficient,
ε = Venturi expansion factor,
D_1 = Venturi upstream internal diameter,
D_2 = Venturi throat internal diameter,
$\Delta p_{venturi}$ = Differential pressure between upstream and throat of the venturi, and
ρ = Air density.

The expansion factor (ε) depends on the Von Karman constant (K) whose value was not available at the time of this study. Therefore, to simplify the calculations, the discharge coefficient (C_{VD}) and the expansion factor (ε) were replaced by a single coefficient C (calibration constant) in Equation 3.2. The air speed (u_g) in the conveying line was obtained from dividing the corresponding Q_m by the cross-sectional area of the acrylic tube in the conveying line (Equation 3.3):

$$Q_m = C \ \frac{1}{4} \ \pi \ D_2^2 \ \frac{1}{\sqrt{1 - \left(\frac{D_1}{D_2}\right)^4}} \ \sqrt{2 \ \Delta p_{venturi} \ \rho} \ , \qquad \textbf{Equation 3.2}$$

where, C = Venturi calibration constant, and

$$u_g = \frac{Q_m}{A} = \frac{Q_m}{\pi \ \frac{D^2}{4}} , \qquad \textbf{Equation 3.3}$$

where,

A = Cross-sectional area of the conveying line, and
D = Diameter of the conveying line (acrylic tube).

Two similar pressure transmitters, $P_{upstream}$ and P_{throat}, were installed to measure the gauge pressure at the upstream and the differential pressure between the upstream and the throat,

respectively. The specifications of the pressure transmitters are given in Table 3.3. The pressure transmitters were calibrated against a standard instrument (details provided in Section 3.5).

Table 3.3: Specifications of the pressure transmitters connected to the venturi meter for measuring the air flow rate.

Make and Model	Measurement Range	Quantity
Dwyer, 616C-5	0-10″ of water column	2

When the door of the (Hardy) lab was open for couple of minutes in winter, the lab temperature changed significantly. To consider the effect of temperature and humidity variation on the air density, a correlation (Equation 3.4) provided by Tsilingiris (2008) was used:

$$\text{Air Density } (\rho) = \frac{1}{z_v}\frac{p_o}{R\,T_v}\,M_a\left[1 - f(P,T)\;RH\left(1 - \frac{M_v}{M_a}\right)\left(\frac{p_{sv}}{P_o}\right)\right], \qquad \textbf{Equation 3.4}$$

where,

z_v = Compressibility factor,

p_o = Absolute pressure at venturi upstream (Pa),

R = Gas constant (8.314 J/ mol-K),

T_v = Temperature inside the venturi (K),

M_a = Molecular mass of dry air (28.97 kg/k-mol),

$f(P,T)$ = Enhancement factor (accounts for a small increase of saturation vapor pressure due to the interaction between the real gas molecules),

RH = Relative humidity of air inside the venturi,

M_v = Molecular mass of water vapor (18.0 kg/k-mol), and

p_{sv} = Saturated vapor pressure (kPa).

The expressions for the variables (z_v, $f(P,T)$, and P_{sv}) in Equation 3.4 are provided in Appendix A. Temperature, humidity, and barometric pressure were measured as was the temperature of the air flowing through the venturi. The humidity was adjusted to the *RH* at venturi air temperature. The specifications of the aforementioned sensors are provided in Table 3.4.

Table 3.4: Specifications of the sensors used for calculating the air density.

Physical Parameter	Make/Supplier	Model	Range
Pressure (room condition)	Freescale Semiconductor	MPXHZ6116A	20 to 115 kPa
Temperature and humidity (room condition)	Measurement Specialties	HTM25X0LF	-20 to 70°C
Temperature (inside the venturi)	Epcos	Thermistor 57861	-55 to 155°C

3.1.3 Fan control system

An automated control system was in place to control the fan speed in order to maintain the air flow rate close to the target value. This system continuously compared the measured air flow rate (by the venturi) and the target air flow rate (provided by the user). Based on the difference between the measured and the target air flow rates, a control signal was sent to the fan unit to take the corrective action (speed up or slow down or maintain the same fan speed), so that the difference in measured and target air flow rates could be minimized.

The fan control system had a DAQ (data acquisition unit), named as *D-1*, which received the output signals from the pressure transducers (installed with the venturi) and the other sensors listed in Table 3.4. *D-1* (Model: NI USB-6009) transmitted those signals to a computer program[1] (developed in LabVIEW[2]), named *Fan Controller*, which was programmed to process the signals and to calculate the air density and the air flow rate (equations mentioned in Section 3.1.2). The computer program then compared the calculated air flow rate with the target (provided by the user), and accordingly instructed the VFD in the fan unit to adjust the frequency and voltage

[1] Developed by Dr. S D Noble, T Keep, and L Mittal
[2] National Instruments, Austin TX

driving the fan motor to control its speed. This loop continued until the data collection (for 60 s) was complete.

3.2 Solid material (wheat) storage and metering system

The experiments in this study were conducted for the pneumatic conveying of the wheat grains at different operating conditions. The dimensions[3] of the wheat grains are provided in Table 3.5.

Table 3.5: Dimensions of the wheat grains used in this study.

Shape	Spheroid
Equivalent spherical diameter	4.05 mm
Aspect ratio	2.3

The grains were stored in a steel tank (placed on a mobile cart) having a secure lid on the top which could be opened to refill the tank whenever desired. A metering system at the bottom of the tank dispensed the grains from the tank to the conveying line (Figure 3.5). The grains dispensed by the metering system were delivered to the conveying line through a tube inclined at 45˚ from the vertical.

[3] Documented by J. Gervais.

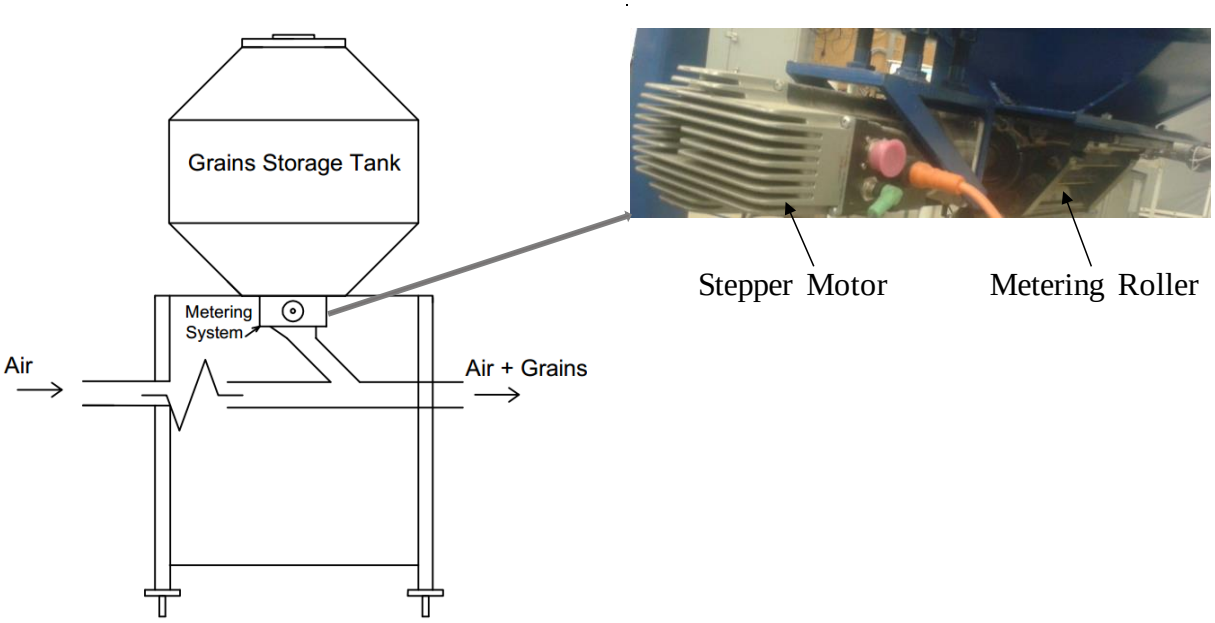

Figure 3.5: Wheat grains storage tank and metering system. The inset shows the picture of the metering system.

The metering system, consisting of a feed roller powered by a stepper motor (MDrive®42AC Plus Motion Control, Schneider Electric; integrated driver; 51200 steps per revolution), dispensed the wheat grains from the storage tank to the conveying line. The motor had a reducing gearhead on its output shaft, and the feed roller had 10 identical straight flutes over its periphery.

The speed of the roller for a target supply rate of grains was obtained from its calibration curve[4]. The desired speed, in rotations per minute (RPM), of the roller was entered by the user in the designated tab on the front panel of *Data Acquisition* program (refer to Section 3.4), which communicated this input value to the controller of the stepper motor. In this study, three different

[4] Documented by T Keep on 2013-10-11

feed rates of grains were used: 20 g/s, 60 g/s, and 100 g/s with corresponding roller speeds of 10, 30, and 50 RPM, respectively.

3.3 Conveying line (pipe)

The experimental setup had a 11.1-m-long horizontal conveying line (pipe) through which the grains (dispensed by the metering system) were transported by the air to the collection bin (at the exit). The pipe was laid 0.35 m above the ground and was supported by steel arms, jack stands, and a wooden platform. The pipe was made in three different sections: the first and the last sections were made of transparent and rigid acrylic tubes. To create a bend in the pipe, the middle section was built from a flexible and semi-transparent PVC tube (Figure 3.6). This section (PVC tube) had a slightly larger ID such that it fit snuggly on the acrylic tube sections (first and last) at both ends. All of the tube joints were properly sealed and secured using tape, glue, and pipe clamps. The specifications of the aforementioned three pipe sections are provided in Table 3.6.

To study the effect of the pipe layout on the grain flow condition inside the pipe, five different pipe layouts were tested in this study. The layout of pipe was changed in the horizontal plane itself by changing the bend angle in the middle section (PVC tube) of the pipe, as shown in Figure 3.7. The five bend angles tested in this study were: 0.0° (straight pipe), 22.5°, 45.0°, 67.5°, and 90.0° (Figure 3.1). A bend radius of 0.64 m was used for all bends.

Table 3.6: Specifications of the sections in the conveying line (pipe).

Pipe Section	Material	Nature	ID	Cross-Sectional Area	Total Length
Section 1	Acrylic	Rigid and transparent	57.35 mm	2583.19 mm^2	6.5 m
Section 2	PVC	Flexible and opaque	63.98 mm	3214.98 mm^2	1.6 m
Section 3	Acrylic	Rigid and transparent	57.35 mm	2583.19 mm^2	3.3 m

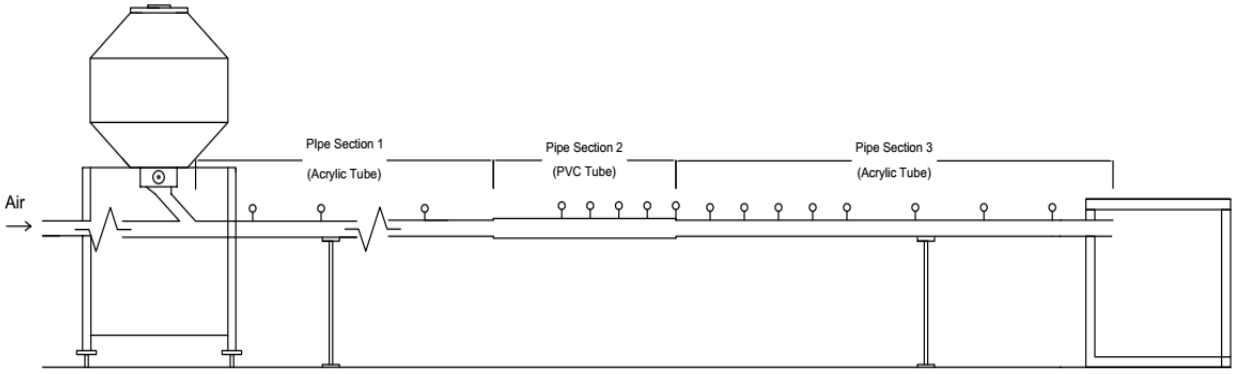

Figure 3.6: Schematic diagram of the different layouts of the conveying line (pipe) used in this study.

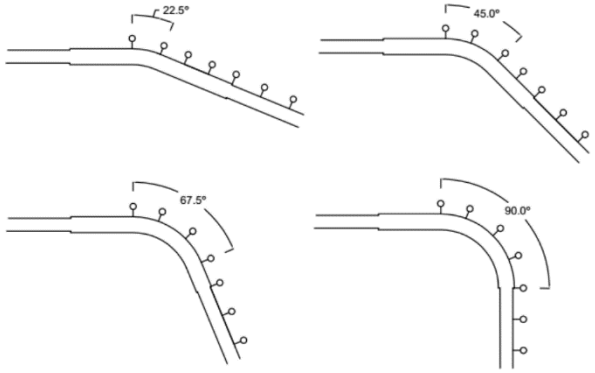

Figure 3.7: Schematic of the bends (22.5°, 45.0°, 67.5°, and 90.0°) which were created in flexible PVC section of the conveying line.

3.3.1 Pressure measurement

One of the main objective of this study was the analysis of the pressure drop along the pipe in all tests conditions. In this context, the pressure drops in 15 different sections of the pipe were measured by the pressure transmitters whose specifications are summarized in Table 3.7.

Table 3.7: Specifications of the pressure transmitters installed in the experimental setup to measure the pressure drop in different sections of the conveying line (pipe).

Make and Model	Measurement range	Quantity
Dwyer, 648B-4	0-1″ of water column	12
Dwyer, 616C-1	0-3″ of water column	2
Dwyer, 616C-3	0-10″ of water column	1

The pressure taps were installed over the small holes on the top surface of the pipe and perpendicular to the pipe wall. The 2.0 mm diameter holes were drilled by drill bit and the plastic barbs (taps) were glued/cemented around the holes. Due to the difference in their outer surfaces, the acrylic and PVC tubes required different methods for installing the pressure taps. For the acrylic tubes, the holes were drilled first, and then T-shaped plastic barbs were glued and sealed to the pipe using silicone caulking. For the PVC tube, a slightly different method was required due to its ridged outer surface. As these ridges did not allow plastic barbs to sit on the hole and seal it properly, 30-mm-long pieces of flexible PVC tubing (4.76 mm ID) were inserted between the two helixes prior to drilling the holes. PVC cement was used to join the tubes and was allowed to cure for a about 30 hours. Once cured, a small hole of 2.0 mm diameter was drilled by a drill bit in the PVC tube (conveying line) by accessing the conveying line through the flexible hose. A soap water test was performed to ensure that there was no leakage of the air from any of the pressure taps. The aforementioned two types of pressure taps are shown in Figure 3.8.

(a) Tap on acrylic tube (b) Tap on PVC tube

Figure 3.8: Image of the pressure taps in the conveying line.

3.4 Data collection unit

The pressure transmitters, installed along the pipe, sent their output signals to a DAQ (data acquisition unit), named *D-2* (Model: NI 9203). The DAQ (*D-2*) further transmitted those signals to a computer program (developed in LabVIEW), named as *Data Acquisition*, which was programmed to process those signals and to record the data. The data for each test were recorded for 60 s, during which approximately 240 data points (for each parameter) were recorded. For ease in data sorting, data were recorded in two designated files: *Raw* (transient data of 60 s) and *Mean* (average of the transient data for 60 s).

The *Fan Controller* program (refer to Section 3.1.3) was also in parallel communication with the *Data Acquisition program,* to which it transferred all the data that it processed from the signals coming through DAQ *D-1*. Thus, the data from both DAQs *D-1* and *D-2* were recorded in the designated files: *Raw* and *Mean.*

3.5 Calibration of instruments

3.5.1 Pressure transmitter calibration

Pressure transmitters were calibrated in-house against a pressure calibrator (make-GE, model- DPI 605) having an operating range of -1 to 20 bar. The accuracy of the calibrator for the operating range (0.000 to 0.249 bar) of the pressure transmitters installed in the experimental setup, was ±0.00015 bar (or ± 15 Pa). The calibration had two steps for adjustment: zero and full scale. At zero, both ports (high and low) of the pressure transmitter were connected to two pressure taps in the conveying line. At full scale adjustment, the high pressure port was connected to the calibrator and the low pressure port was connected to the conveying line. The span was adjusted with ±0.0002 bar accuracy.

3.5.1.1 Venturi calibration

The venturi was calibrated using a Pitot-static probe to traverse the outlet of a long section of pipe. The Pitot-static probe was mounted at the open end of a steel pipe (ID 120 mm) whose other end was connected to another pipe in which the venturi was installed. Two pressure transmitters (specifications provided in Table 3.8) were connected to the Pitot-static probe to measure the static pressure and the velocity pressure at the outlet of the steel pipe. The air speed at the pipe outlet was calculated by using Equation 3.5:

$$v = 1.291 \sqrt{\frac{1000}{B} \; \frac{T_0}{289} \; \frac{100000}{100000 + p_{static}} \; p_{velocity}} \;, \qquad \textbf{Equation 3.5}$$

where,

v = Air speed measured by Pitot-static probe (m/s),
B = Barometric pressure (Pa),
T_0 = Room air temperature (K),
p_{static} = Static pressure at steel pipe outlet (Pa), and
$p_{velocity}$ = Velocity pressure at steel pipe outlet (Pa).

Table 3.8: Specifications of the pressure transmitters connected to the pitot-static probe to measure the static pressure and the velocity pressure for calculating the air speed.

Parameter	Make / Model	Measurement range	Quantity
Static pressure	Dwyer, 616-1	0-3" of water column	1
Velocity pressure	Dwyer, 616-2	0-6" of water column	1

The calibration data (i.e. the air speed measured by the venturi and the Pitot-static probe) were collected for 21 different air flow rates which were regulated by changing the fan speed from a manual control. For every tested fan speed, the Pitot-static probe was traversed at 48 locations along two diameters of the steel pipe to measure the air speed at the selected locations (Figure 3.9).

The distance between two consecutive traverse locations was 5 mm. The resultant air speed in the steel pipe was obtained by the area-weighted integration from the 48 values collected for the corresponding air flow rate. Similarly, the venturi also measured and averaged out 48 air speeds for each of the tested 21 fan speeds. The data of the air speeds measured by the venturi and the Pitot-static probe were plotted and a linear trend line equation was obtained. This trend line equation was incorporated in *Fan Controller* program (refer to Section 3.1.3) which finally provided the actual air speed.

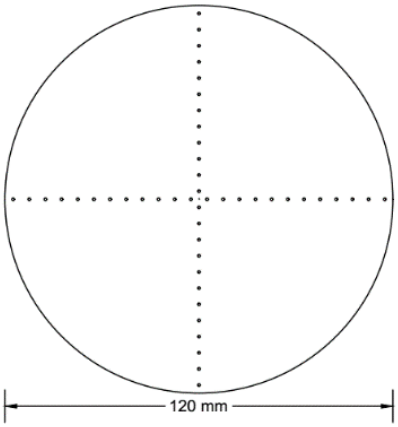

Figure 3.9: Cross-sectional view of the steel pipe (ID 120 mm) on which the Pitot-static probe was mounted for the venturi calibration. The traversing points along the horizontal and vertical diameter have also been shown.

Chapter 4 : Results and Discussion

In this study, tests of pneumatic conveying of wheat grains through a 11.6-m-long horizontal conveying line (or pipe) were conducted over a wide range of operating conditions. Table 4.1 provides a summary of the test conditions that were created by manipulating three operating variables: the pipe layout (bend angle θ), grain feed rate ($\dot{m}_p$), and air speed (u_a).

Table 4.1: Summary of the tests conducted for the pneumatic conveying of wheat grains through a horizontal pipe.

Pipe layout				
	Bend angle (θ)	**$\dot{m}_p$= 20 g/s**	**$\dot{m}_p$= 60 g/s**	**$\dot{m}_p$= 100 g/s**
Straight pipe	0.0°	Max: 16.0 m/s Min: 6.5 m/s (18 air speeds)	Max: 20.0 m/s Min: 9.5 m/s (19 air speeds)	Max: 21.0 m/s Min: 13.0 m/s (14 air speeds)
Bent pipe	22.5°			
	45.0°			
	67.5°			
	90.0°			
Number of test conditions		90	95	70
Number of replicates		x3	x3	x3
Sub-total of tests		270	285	210
Total number of tests			765	

For each of the pipe layouts and grain feed rates, the tests proceeded from high to low air speed. Each of the tests had a total duration of 180 s. The test began with air only flow at the target rate and continued for 60 s so that the fan and the air speed could stabilize. Then, the metering system was switched on and the air-grain flow stabilized for another 60 s. Finally, the data collection was also started which completed in the following 60 s. After each test (i.e. data collection for an air speed), the grain supply was stopped and the air flow continued until the pipe was cleared of product. This data collection methodology was followed to keep the data of each test independent and unaffected by the previous test condition. The same process was repeated for all 765 tests.

Approximately 240 data points for every measured parameter were acquired during the 60 s of data collection. The average of the 60 s of data was used for the analysis in this study. Also, the data from three repetitions of each test were averaged together, unless otherwise indicated. There was almost a negligible difference ($\leq$ 0.04 m/s) between the target and actual air speed during the tests (for air speeds equal to and higher than the settling speed). Therefore, for a clear presentation of results, the target air speeds were considered for the data analysis.

The data analysis provided the results highlighting the effectiveness of the pressure drop per unit length (pressure gradient) in identifying the flow conditions of the grains (especially settling in the pipe) during the conveying process. Following are the main points of the discussion in this chapter:

- Flow pattern of grain at various air speeds;
- Settling pattern of grain at various grain feed rates and pipe layouts (straight and bent); and
- Utility of the average and the local pressure gradient for identifying the flow condition of the grains.

4.1 Flow pattern of wheat grains at various air speeds during pneumatic conveying of wheat grains

The tests were conducted over a wide range of air speeds. Starting from the highest air speed in the range, in sequential steps, the tests proceeded towards the lowest speed. The flow was visually observed through the transparent wall of the pipe. A sketch in Figure 4.1 illustrates the flow pattern of grains appeared at different levels of air speed during the tests.

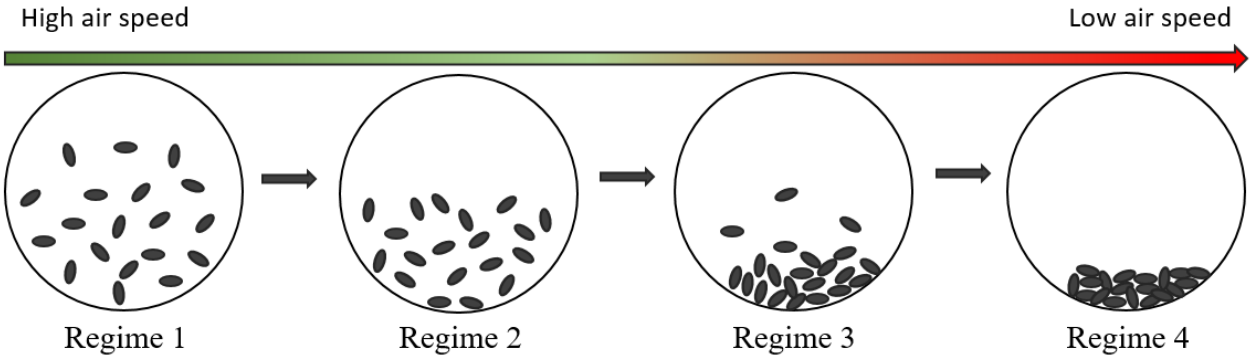

Figure 4.1: A sketch illustrating the flow pattern of wheat grains in the cross section of horizontal pipe during the pneumatic conveying tests at various levels of air speed.

At high air speeds, the grains were suspended in air, however not homogenously, as the majority of grains were flowing in the lower half of pipe (Regime 1). As the air speed was reduced, the concentration of grains moved further towards the pipe bottom (Regime 2), and in the continuation of air speed reduction, a condition arrived when the grains were not suspended at all and were moving in the form of layers and groups on the bottom of pipe (Regime 3). Upon further decreasing the air speed, the grains initially slid on the bottom of pipe for short distances and then stopped and settled down before reaching the pipe exit (Regime 4).

The air speed at which the grains permanently settled down in pipe is termed here as the settling speed (u_{set}). At the settling speed, the grains at first, slid approximately 6.6 m to 8.3 m, and then settled down in the pipe. Upon going below the settling speed, the settling location shifted slightly upstream at every next lower air speed. The flow behavior indicated that the visual monitoring of flow conditions could indicate if the operating air speed was too close or far from the settling speed, and could be useful in maintaining the air speed according to the real-time requirement.

In the following sections, the discussion is first focused on the effect of the pipe bend angles and the grain feed rate on the settling speed. This is followed by an explanation of the characteristics of the pressure gradient data and its usefulness in identifying u_{set} and the optimal air speed for the conveying process.

4.2 Effect of pipe layout and grain feed rate on settling speed and air-flow requirement

Initially, it was suspected that the settling speed should see an increase at every higher grain feed rate ($\dot{m}_p$) and/or every larger bend angle (θ) in the pipe. This assumption was based on the understanding that in both of these cases (increase in $\dot{m}_p$ and/or θ), the interactions of the grains with the air, the pipe, and among themselves would increase significantly, and thus would result in more significant energy losses and fluctuations in the air speed. Therefore, to avoid settling conditions at the bend and/or at higher grain feed rates, the air flow would likely need to be maintained at a higher air speed.

The results in Table 4.2, however, show that though the u_{set} increased with the increase in grain feed rate, u_{set} did not change noticeably with the increase in bend angle (except for a marginal decrease in settling speed for θ = 90.0° and $\dot{m}_p$= 20 g/s).

Table 4.2: Settling speed (u_{set}) obtained from the tests conducted for the pneumatic conveying of wheat grains, at various grain feed rates ($\dot{m}_p$), through a horizontal pipe laid out in various configurations (θ).

Conveying Line			Settling speed (u_{set}) [m/s]		
Layout	**Bend angle (θ)**	**Repetition**	**$\dot{m}_p$ = 20 g/s**	**$\dot{m}_p$ = 60 g/s**	**$\dot{m}_p$ = 100 g/s**
Straight Pipe	0.0°	1	10.5	12.5	13.5
		2	10.5	12.5	13.5
		3	10.5	12.5	13.5
Bent Pipe	22.5°	1	10.5	12.5	13.5
		2	10.5	12.5	13.5
		3	10.5	12.5	13.5
	45.0°	1	10.5	12.5	13.5
		2	10.5	12.5	13.5
		3	10.5	12.5	13.5
	67.5°	1	10.5	12.5	13.5
		2	10.5	12.5	13.5
		3	10.5	12.5	13.5
	90.0°	1	10.0	12.5	13.5
		2	10.0	12.5	13.5
		3	10.0	12.5	13.5

The reason for the particular observation in one case (θ = 90.0° and $\dot{m}_p$ = 20 g/s), where u_{set} was obtained lower than the other test conditions, is not clear. However, the reproducible measurement of settling speed (in all three repeats) suggests that it can be used as a dependable process parameter in pneumatic conveying processes. The most probable reason for not observing a change in settling speed was the use of the *fan controller* system (refer to Section 3.1.3) which kept the air flow rate constant through out the process irrespective of the pipe layout and internal flow conditions. This possibly did not let the flow slow down to an extent where the grains could start settling down. This observation highlighted the significance of using a *fan controller* in the conveying system which can make the pipe layouts insignificant to the grain flow characteristics. Also, another responsible factor seemed to be the large radius of bend $\left(\frac{\text{Radius of bend}}{\text{Radius of pipe}} = 20\right)$ which was used in this study. Additional tests would be useful to further examine if the effect of a bend

remains similarly insignificant with using the *fan controller* even for a smaller bend radius $\left(\frac{\text{Radius of bend}}{\text{Radius of pipe}} < 20\right)$ and/or higher grain feed rate ($\dot{m}_p$ > 100 g/s).

As discussed above, settling speed increased with an increase in the grain feed rate. However, the settling speed did not increase in proportion to grain feed rate. In other words, less conveying air was required per unit mass of grains as the solid feed rate was increased. Figure 4.2 shows a trend of air flow rate at settling speed *vs.* grain feed rate. This seems to be an important feature in the conveying process where optimization of the load carrying capacity of air is of particular interest.

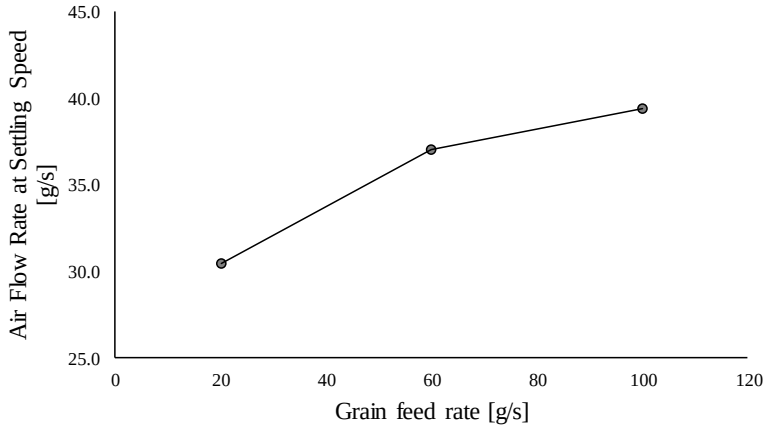

Figure 4.2: Air flow rate at settling speed *vs.* grain feed rates.

4.3 Average pressure gradient across the entire length of straight pipe at various grain feed rates and pipe layouts

As mentioned in Chapter 2, some studies previously showed that the trend of pressure gradient (pressure drop per unit length of pipe) could indicate flow conditions of conveyed solid particles inside the pipe. These findings opened up the possibilities for using the pressure gradient data to obtain important process parameters like optimum air speed and settling speed for a process. However, it is noteworthy that the physical properties (e.g., shape, size, and density) of the solid

material can greatly influence the overall flow pattern in the conveying process. Some previous studies presented experimental data (pressure gradient vs. air speed) for the pneumatic conveying of various solid materials, however, none of them conducted the tests with wheat grains. The current study attempts to fill this gap by collecting and analyzing pressure gradient data for pneumatic conveying of wheat grains (aspect ratio ~ 2.3:1).

Hereinafter, the pressure gradient [Pa/m] or the pressure drop per unit length of pipe $\left(\frac{\Delta p}{\Delta L}\right)$ is represented by the symbol ΔP. Different subscripts are used with the symbol ΔP for clear representation of pressure gradient in different sections of the pipe.

4.3.1 Straight pipe

The schematic of the straight pipe layout is shown in Figure 4.3. The data of average pressure gradient (ΔP_{avg}) across the entire length of straight pipe are presented by plotting it against u_g, as shown in Figure 4.4. The average of three trials of each test have been used for the analysis. The standard deviation of three trials of the tests is shown by the error bar; and for better visualization of ΔP_{avg} trend at high and low air speeds, ΔP_{avg} data at low air speeds (below settling speed) have been presented by the scattered data points. To highlight the pressure gradient when the grains settled in pipe (at settling speed), the respective data points are demonstrated by red square markers.

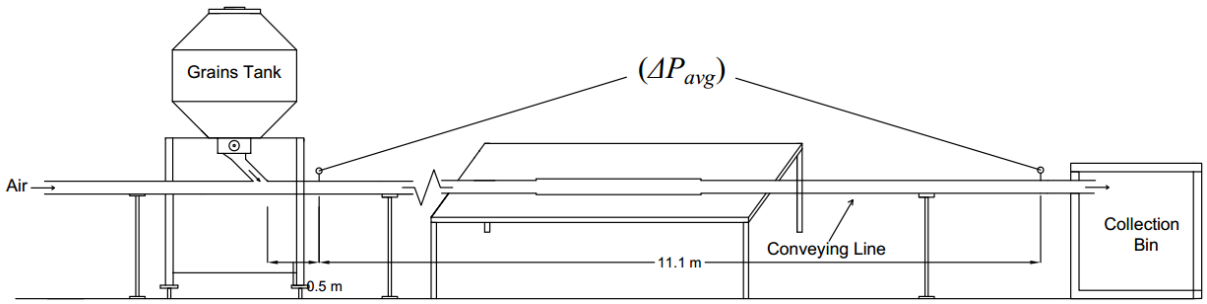

Figure 4.3: Schematic of the straight pipe layout with pressure taps measuring the average pressure gradient (ΔP_{avg}) across the entire pipe in pneumatic conveying of wheat grains.

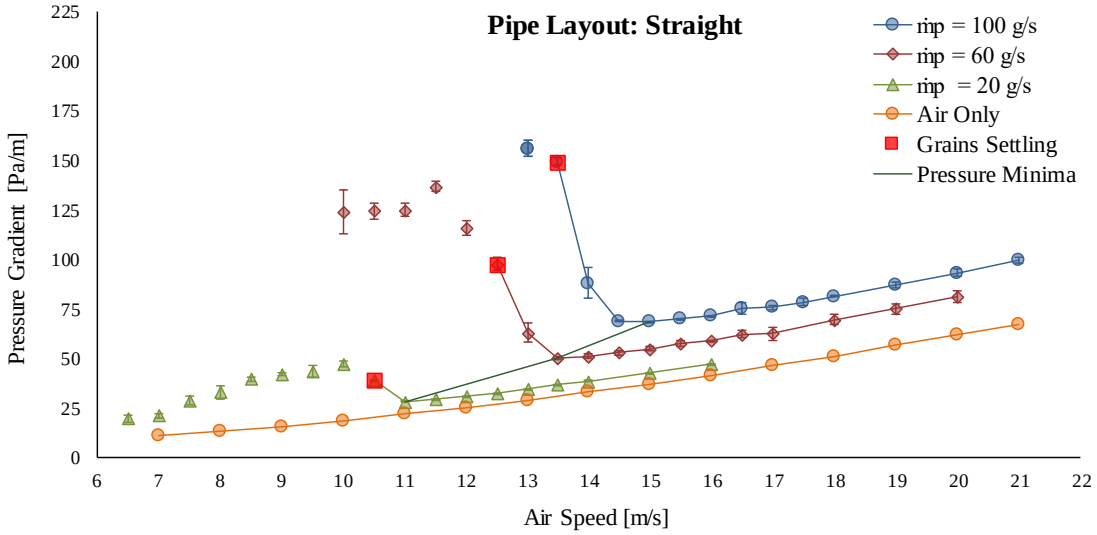

Figure 4.4: Average pressure gradient (ΔP_{avg}) over a range of air speed (u_g) across the entire straight pipe for the grain feed rate ($\dot{m}_p$) of 0 g/s (air only), 20 g/s, 60 g/s, and 100 g/s.

The qualitative trend of ΔP_{avg} was quite similar to those presented in previous studies (for conveying different kinds of materials). The pressure drop in air only flow ($\dot{m}_p = 0$) was mainly caused by the frictional losses between the pipe wall and air flow. With a decrease in air speed, a lesser amount of air came in contact with the pipe wall, causing lesser frictional loss between the air and the pipe wall. Hence, as expected, ΔP_{avg} for the air only flow was found to decrease monotonically with the air speed. On the other hand, resistance to the flow with grains ($\dot{m}_p \neq 0$)

was not only caused by the friction between the air and the pipe wall, but also due to the drag force offered by the grains and the grain-grain collisions. As a result, ΔP_{avg} for the flow with grains ($\dot{m}_p \neq 0$) was always higher than that in the air only flow.

At high air speeds, the grains were distributed all across the cross-section of the pipe and their (grains) mutual collisions were limited (Regime 1 in Figure 4.1). Thus, the contribution of the grains to the overall pressure drop (or average pressure gradient) was only minimal; and the frictional loss (between the air and the pipe wall) was the dominant factor for causing the pressure drop. As a result, at high air speeds, ΔP_{avg} consistently decreased upon reducing the air speed, but only until reaching the minimum value of ΔP_{avg}. The air speed corresponding to the minimum value of ΔP_{avg} is termed here as the critical speed (u_{cr}). Also, while reducing the air speed from the high end to the critical speed (i.e. $u_g \geq u_{set}$), the flow behaviour changed from Regime 1 to Regime 2 (Figure 4.1) at some intermediate air speed. Upon any further reduction in the air speed ($u_g < u_{set}$), the concentrated grains in the lower half of the pipe began to form moving layers (Regime 3 in Figure 4.1). In this condition, the higher concentration of grains in the lower half of the pipe and the increase in mutual collisions caused excessive energy loss and thus resulted in the increase in the pressure gradient (as compared to that at previous higher air speed). Upon further reduction in air speed, the pressure gradient continued to increase until the grains started settling down (or the settling speed arrived).

At very low air speeds ($u_g \ll u_{set}$), the trend of ΔP_{avg} was inconsistent, but in general ΔP_{avg} started decreasing again with the decreasing air speed (similar to the case of $u_g \geq u_{cr}$). The possible reason behind this trend was, that at such low air speeds, the grains could not travel much farther from the feeding point, and eventually settled down. Therefore, the flow condition could apparently be considered as the air only flow in most of the downstream part of the pipe. This

indicates that for $u_g \ll u_{set}$, the pressure drop was mainly due to the frictional loss (between the air and the pipe wall) which consistently reduced at further lower air speed and getting past the restriction.

For all three grain feed rates, the overall trend of ΔP_{avg} was qualitatively very similar, except that the ΔP_{avg} curves shifted upwards right with an increase in grain feed rate ($\dot{m}_p$). This basically indicated the higher pressure drop due to larger number of grains in the flow. The critical speed (u_{cr}) and the settling speeds (u_{set}) also increased (however not much) with an increase in grain feed rate ($\dot{m}_p$). It is noteworthy that the settling speed (u_{set}) was consistently lower than the critical speed (u_{cr}) across all the conditions. The small size of the error bars (standard deviation of the data from three trials) at high air speeds ($u_g \geq u_{cr}$) indicated the overall stability and reproducibility of the flow conditions. At low air speeds ($u_g < u_{cr}$), the larger error bars resembled the flow instability due to the ongoing difficulty of air to keep pushing the grains in those conditions.

4.3.2 Bent pipe

This section presents the results for the bent pipe at four different bend angles (22.5°, 45.0°, 67.5°, and 90.0°). Figure 4.5 shows a schematic for the pipe bent at a 90.0° angle (the other three angles of bend were also formed in a similar way). Results for the average pressure gradient for the various bend angles are shown in Figure 4.6.

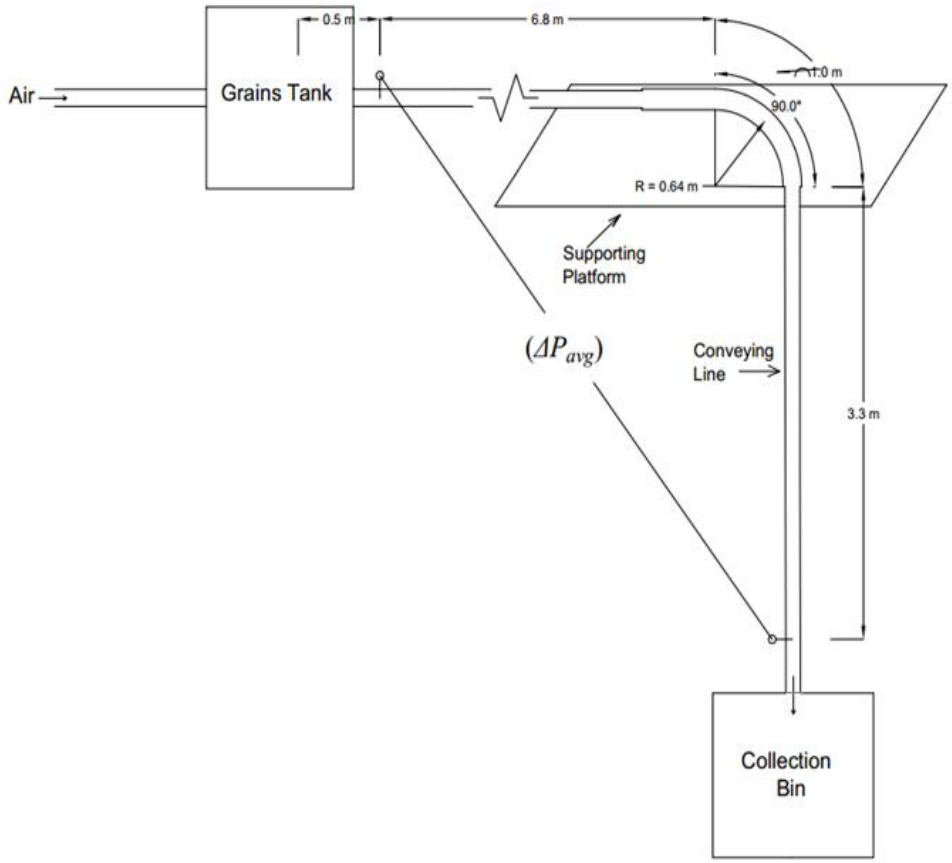

Figure 4.5: Top view schematic of the pipe layout with a 90.0° angle bend for measuring the average pressure gradient (ΔP_{avg}) across the entire pipe in pneumatic conveying of wheat grains.

(a)

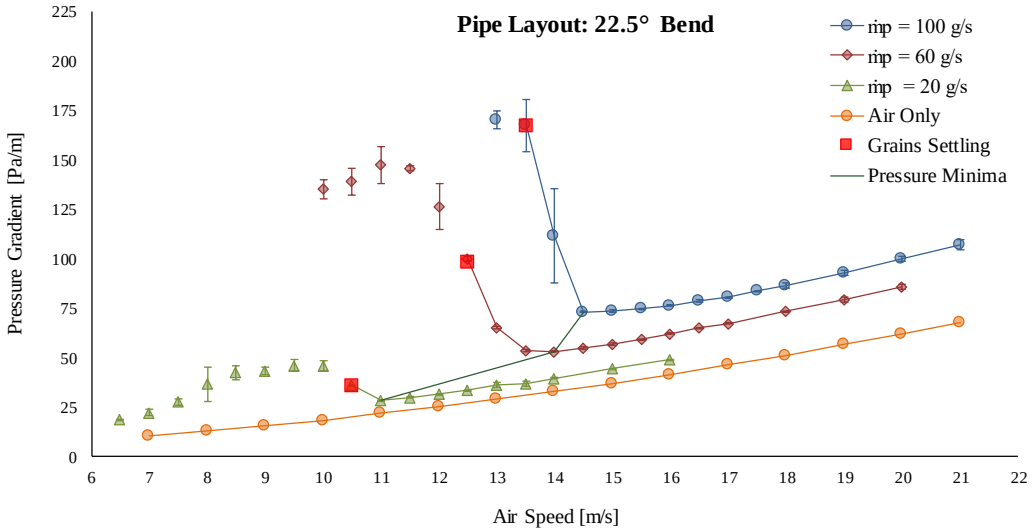
Pipe Layout: 22.5° Bend
ṁp = 100 g/s
ṁp = 60 g/s
ṁp = 20 g/s
Air Only
Grains Settling
Pressure Minima
Pressure Gradient [Pa/m]
Air Speed [m/s]

(b)

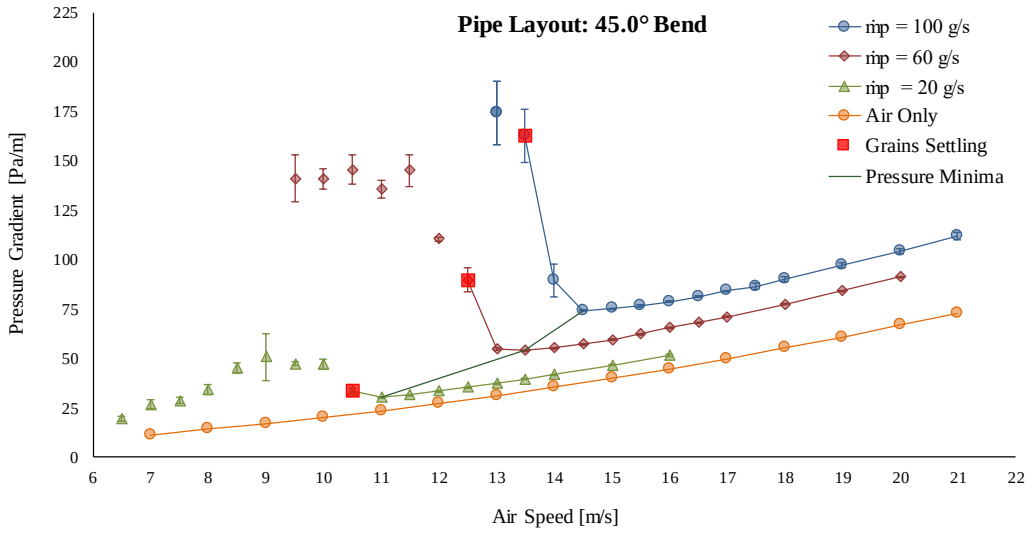
Pipe Layout: 45.0° Bend
ṁp = 100 g/s
ṁp = 60 g/s
ṁp = 20 g/s
Air Only
Grains Settling
Pressure Minima
Pressure Gradient [Pa/m]
Air Speed [m/s]

(c)

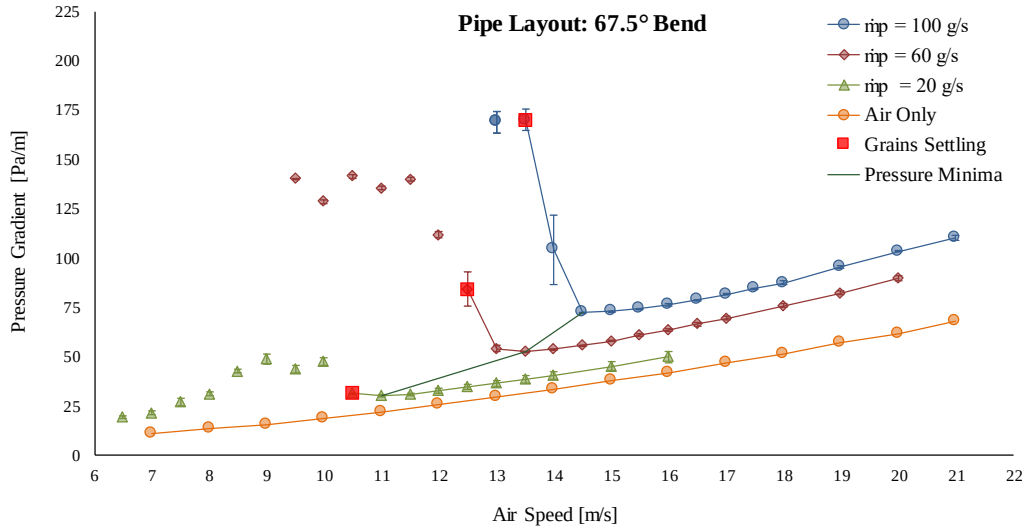
Pipe Layout: 67.5° Bend
ṁp = 100 g/s
ṁp = 60 g/s
ṁp = 20 g/s
Air Only
Grains Settling
Pressure Minima
Pressure Gradient [Pa/m]
Air Speed [m/s]

(d)

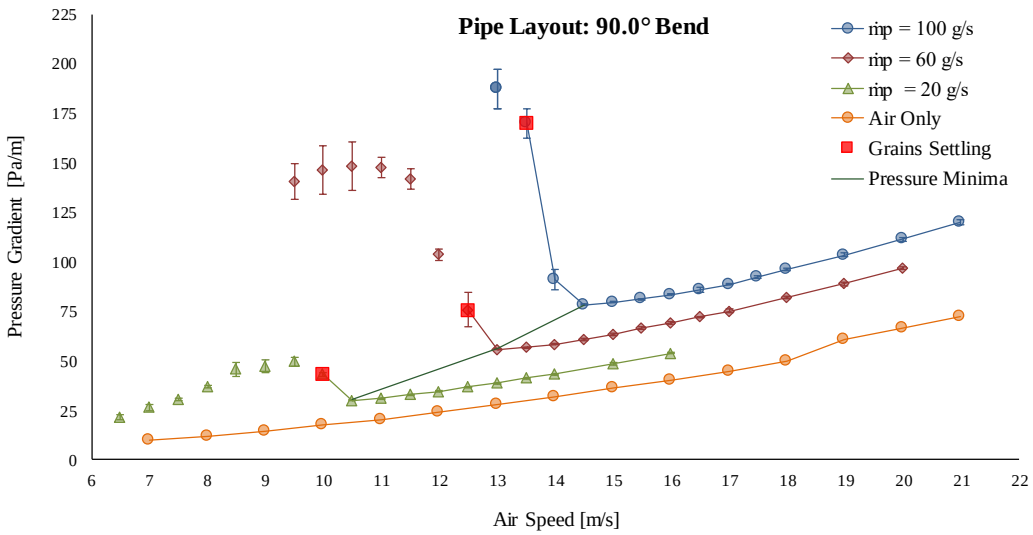

Figure 4.6: Average pressure gradient (ΔP_{avg}) over a range of air speed (u_g) across the entire bent pipe for the grain feed rates ($\dot{m}_p$) of 0 g/s (air only), 20 g/s, 60 g/s, and 100 g/s: (a) 22.5° bend angle, (b) 45.0° bend angle, (c) 67.5° bend angle, and (d) 90.0° bend angle.

The trends of ΔP_{avg} obtained for all of the tested pipe layouts (straight and bent) were qualitatively consistent. This indicated that the change in pipe layout did not significantly affect either flow-behaviour or pressure gradient-trend. Hence, the characteristics of the pressure gradient trend for a straight pipe can also be equally relevant for a bent pipe ($0° \leq \theta \leq 90°$).

As per the visual observations, for $u_g > u_{cr}$, the grains did not settle in pipe not even temporarily, whereas, for $u_{set} < u_g < u_{cr}$, the grains settled in pipe temporarily for few seconds and then just moved ahead with the flow. This pattern indicated that at an air speed right below u_{cr}, the particles tend to settle down in pipe, but the fan controller did not let the air flow slow down and maintained the target air speed in few seconds. That is why the settling was just temporary for few seconds. This indicated the utility of the fan controller in reducing the settling speed by 0.5 to 1.5 m/s in the tested conditions.

Further, it was assumed that ΔP_{avg} in the bent pipe should be higher than that in the straight pipe due to the additional resistance introduced by the bend. Two contributing factors in the

supposed additional resistance are the diversion of flow to an angle, and concentration of grains at the outer-radius wall (due to the centrifugal effect) causing excessive collisions within the bend. This behaviour was expected to be more prominent for larger angles of bend. For illustrating the quantitative effect on ΔP_{avg} due to the presence of a bend in pipe, the data for all five pipe layouts are plotted together in Figure 4.7.

(a)

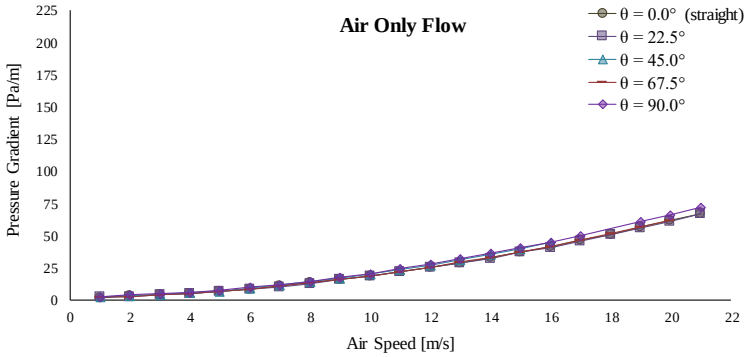

(b)

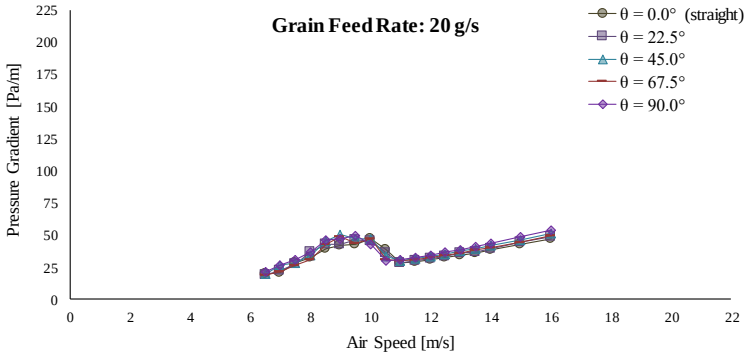

(c)

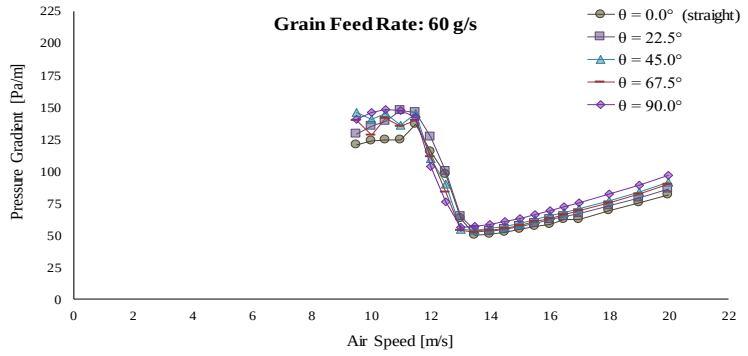

(d)

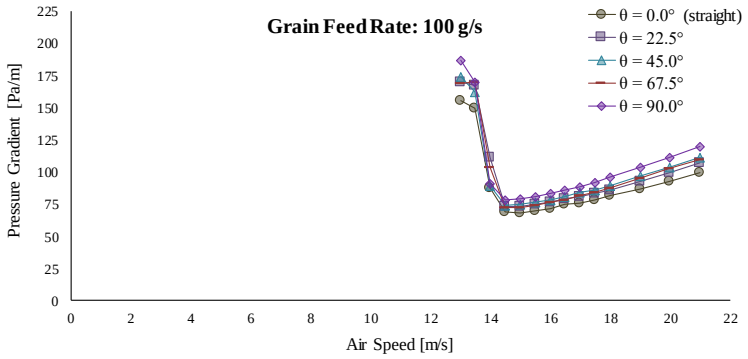

Figure 4.7: Average pressure gradient (ΔP_{avg}) over a range of air speed (u_g) across the entire pipe layout at various bend angles (θ) and for the grain feed rate ($\dot{m}_p$) of: (a) 0 g/s (air only), (b) 20 g/s, (c) 60 g/s, and (d) 100 g/s.

The plotted data showed that for air only flow ($\dot{m}_p = 0$), there is not much difference in ΔP_{avg} upon changing the pipe layout. This indicated that the bend radius was not small enough to significantly affect the pressure drop behaviour for air only flow.

For $\dot{m}_p \neq 0$, At high air speeds, the ΔP_{avg} curves shifted upwards slightly for every next larger angle of bend, indicating the increase in resistance to flow with increase in bend angle. However, the trend was not consistent at low air speeds, perhaps due to high instability in the flow at those conditions. Also, for the 67.5° bend angle, ΔP_{avg} behaved slightly different as it was unexpectedly lower than that for a smaller bend angle of 45.0°. The reason for this observation is not known.

4.3.3 Optimal air speed in pneumatic conveying process

As discussed in previous sections, the trend of ΔP_{avg} was quite consistent across all of the grain feed rates ($\dot{m}_p$) and the pipe layouts. The average pressure drop initially decreased upon reducing the air speed, and this trend continued until reaching a critical speed (u_{cr}) beyond which any further reduction in the air speed resulted in a higher pressure drop (for $u_{set} \leq u_g < u_{cr}$).

Table 4.3: Critical speed (u_{cr}) and settling speed (u_{set}) obtained from the tests conducted for the pneumatic conveying of wheat grains at three grain feed rates ($\dot{m}_p$) through a horizontal pipe bent at five different angles (θ). (The speeds shown here are the mean of the three repetitions of each test.)

Layout	Bend angle (θ)	$\dot{m}_p$= 20 g/s		$\dot{m}_p$= 60 g/s		$\dot{m}_p$= 100 g/s	
		u_{cr} [m/s]	u_{set} [m/s]	u_{cr} [m/s]	u_{set} [m/s]	u_{cr} [m/s]	u_{set} [m/s]
Straight pipe	0.0°	11.0	10.5	13.5	12.5	15.0	13.5
Bent pipe	22.5°	11.0	10.5	14.0	12.5	14.5	13.5
	45.0°	11.0	10.5	13.5	12.5	14.5	13.5
	67.5°	11.0	10.5	13.0	12.5	14.5	13.5
	90.0°	10.5	10.0	13.0	12.5	14.5	13.5

As illustrated in Table 4.3, the critical speed (u_{cr}) was consistently higher than u_{set} by ≤ 1.5 m/s (a detectable difference); u_{cr} therefore seemed to be a strong candidate for being considered as the optimal air speed for the conveying process. Moreover, as the pressure drop corresponding to the critical speed is minimum, high energy efficiency could also be achieved when the air speed is equal to the critical speed (u_{cr}).

The specific position of the critical speed (i.e. corresponding to the minimum of the pressure gradient curve) can conveniently be determined from pre-recorded data of ΔP_{avg} vs. air speed (u_g). Also, the conveying process can be made highly flexible if the critical speed (u_{cr}) can be obtained directly from the real-time process data by lowering the air speed from a relatively high value until the pressure drop starts to increase (which is a signal of $u_g < u_{cr}$). In the future, the feasibility of such an algorithm could also be explored so that it can be implemented as an automated process.

4.4 Local pressure gradient in different sections of the pipe

In a steady flow through a straight and uniform pipe, the local pressure gradient (ΔP_{local}) along any local section of pipe is likely to be similar to the average pressure gradient ΔP_{avg} along the entire pipe. However, in a bent or/and non-uniform pipe, ΔP_{local} may differ significantly from ΔP_{avg}, depending on the geometry and location of the corresponding pipe section. In a bent pipe the local pressure-drop around the bend and along the neighboring downstream sections are expected to be higher than that in rest of the pipe due to high resistance to flow within the bend and reacceleration of flow in the downstream section. The grains slow down in the bent section, and it tends to reaccelerate in the downstream section. Thus, additional energy is transferred from the air in order to reaccelerate the flow in the downstream of bend, resulting in a higher pressure drop.

To understand the effect of the pipe configuration on the local as well as overall flow conditions, the pressure drop was also measured along various local sections along the pipe. The different angles of bend were created in a 1.6-m-long flexible section of the pipe (which was 11.6% larger in diameter than rest of the pipe). To analyze the data for the bent pipe, the local pipe sections are grouped into three major sections: upstream of the bend, the bend, and downstream of the bend. The schematics in Figure 4.8 show the arrangement of the sections and the locations of the pressure transmitters for the straight as well as the bent pipe.

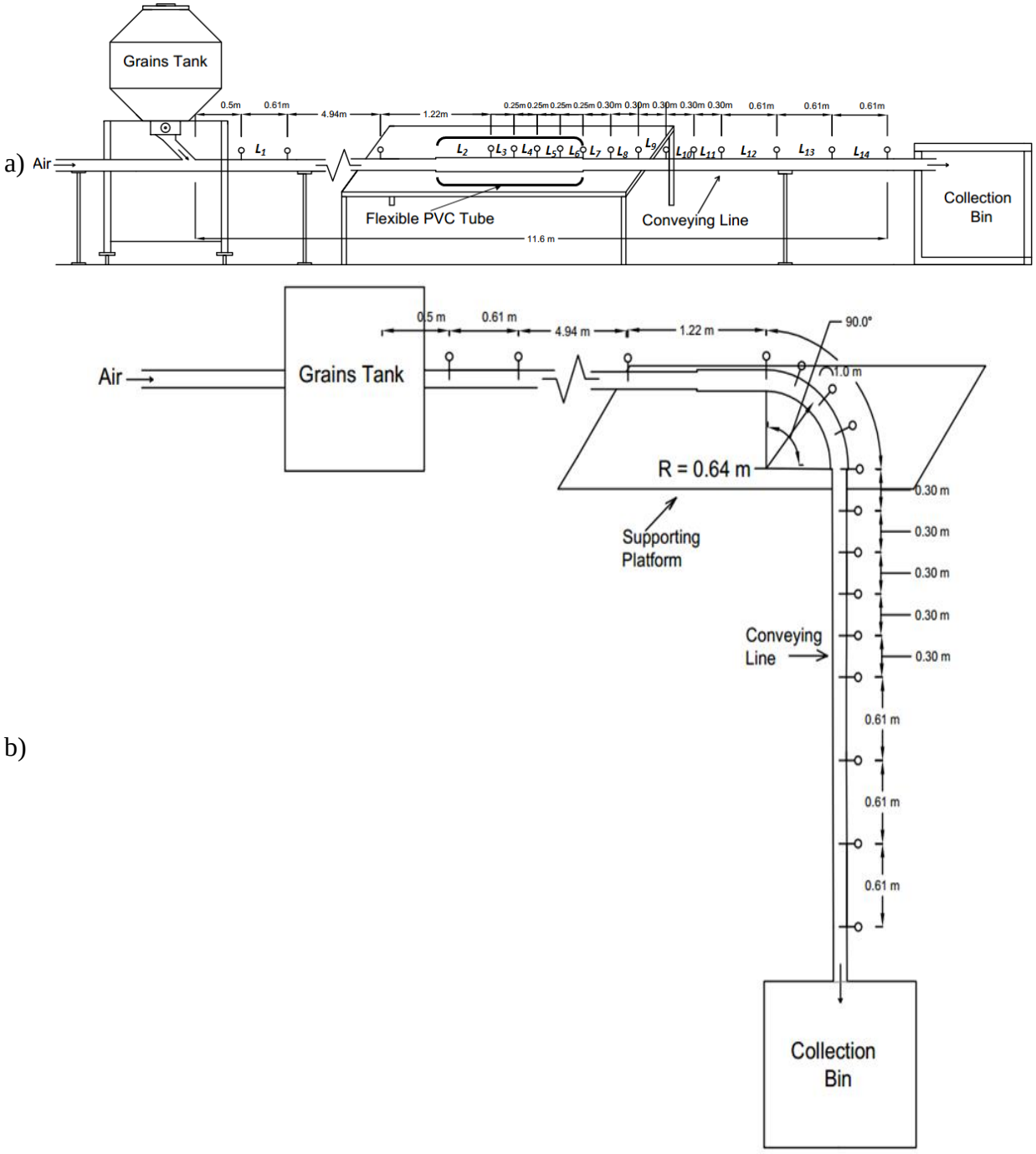

Figure 4.8: Schematic of (a) the straight pipe and (b) the bent pipe (90.0° angle), for the measurement of local pressure-drop in 14 sections along the pipe.

4.4.1 Upstream of the bend

Two pipe sections, L_1 and L_2, were considered for discussing the local pressure gradient (ΔP_{local}) at locations upstream of the bend (Figure 4.8). Because the trends of ΔP_{local} in the

respective sections were qualitatively very similar for all grain feed rates ($\dot{m}_p$) and bend angles (θ), only a limited number of test conditions ($\dot{m}_p$ = 60 g/s and θ = 0°, 45°, and 90°) are provided here (Figure 4.9 for L_1 and Figure 4.10 for L_2). The plotted data for the remaining test conditions are provided in Appendix B. The average pressure gradient ΔP_{avg} for the same test conditions have also been included in the graphs, so that local and average trends of pressure gradient can be compared.

Figure 4.9 shows that the trend of the local pressure gradient ($\Delta P_{local\text{-}L_1}$) along the section L_1 and the average pressure gradient (ΔP_{avg}) along the entire pipe share qualitative similarities at high air speeds.

a)

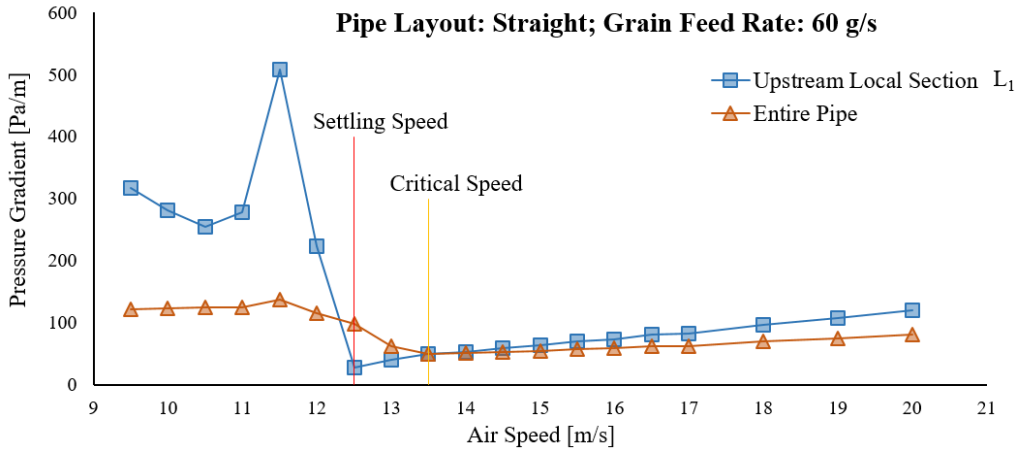

b)

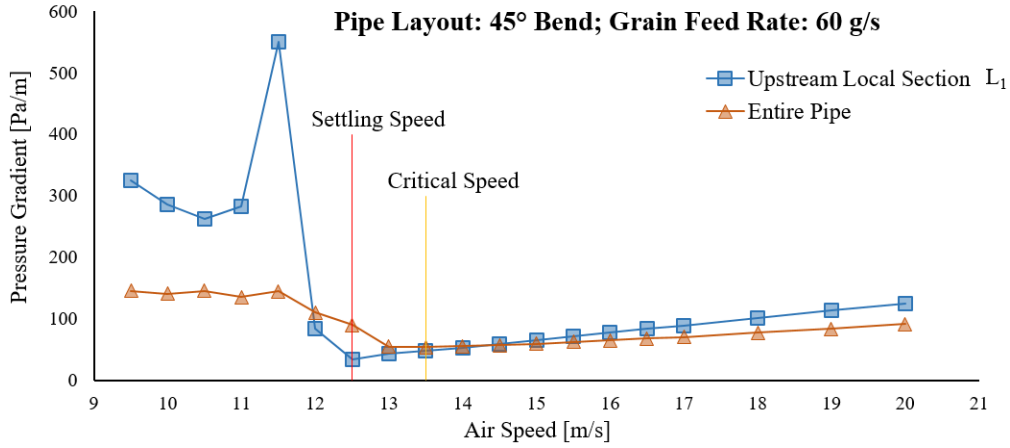

c)

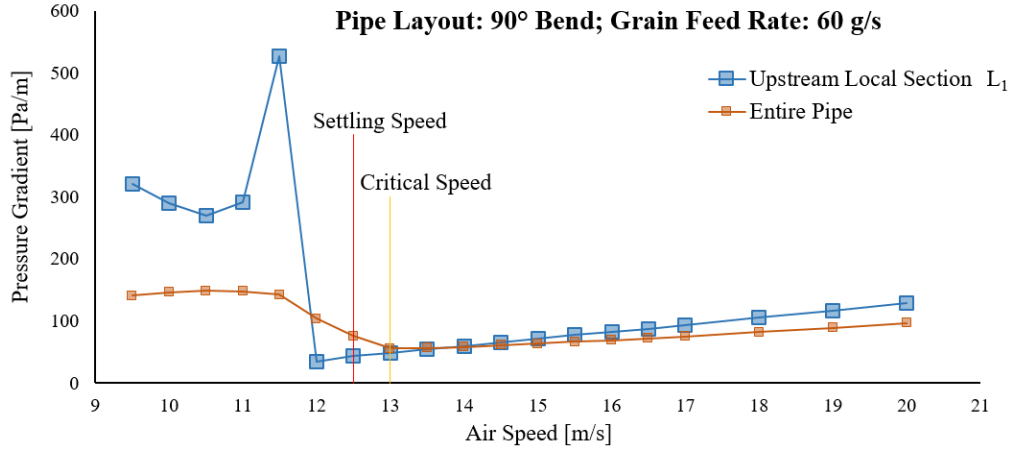

Figure 4.9: Local pressure gradient ($\Delta P_{local\text{-}L_1}$) along the section L_1, and average pressure gradient (ΔP_{avg}) along the whole pipe; for grain feed rate ($\dot{m}_p$) of 60 g/s, and bend angles (θ) of (a) 0.0°, (b) 45.0°, and (c) 90.0°.

At high air speeds, both $\Delta P_{local\text{-}L_1}$ and ΔP_{avg} decreased on lowering the air speed until reaching their respective minimum values. The plots demonstrated that the minima[5] of $\Delta P_{local\text{-}L_1}$ and ΔP_{avg} appeared at different air speeds in each of the test conditions. It was noteworthy that $\Delta P_{local\text{-}L_1}$ kept decreasing with a reduction in air speed even below the critical speed (u_{cr}) and continued this behaviour up to (or sometimes below) the settling speed (u_{set}). This trend was observed because initially (at the settling speed), the settling of grains occurred only downstream of L_1, not in the L_1 section. However, at lower air speeds, the location of settling shifted upstream. When the settling actually occurred in the L_1 section, $\Delta P_{local\text{-}L_1}$ increased rapidly also. This trend indicated that section L_1 was only sensitive to its own local settling, and not to one at settling downstream locations. Therefore, a far upstream section (like L_1) did not seem to be suitable for the purpose of monitoring the overall flow conditions (especially the settling of grains).

Figure 4.10 shows that the trend of the local pressure gradient $\Delta P_{local\text{-}L_2}$ along another upstream section L_2 and the average pressure gradient ΔP_{avg} along the entire pipe also shared many similarities. The trend of $\Delta P_{local\text{-}L_2}$ between the air speed range 13.0 - 20.0 m/s is enlarged as shown in the insets for better visibility.

[5] The air speed corresponding to the minima of ΔP_{avg} is the critical speed (u_{cr}).

a)

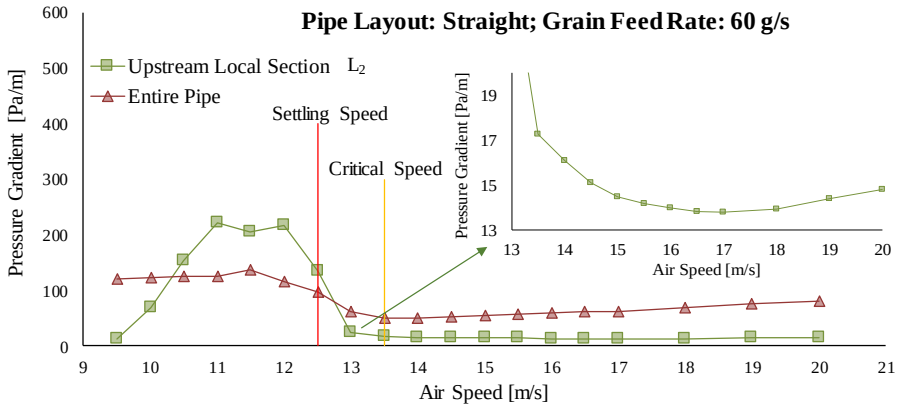

b)

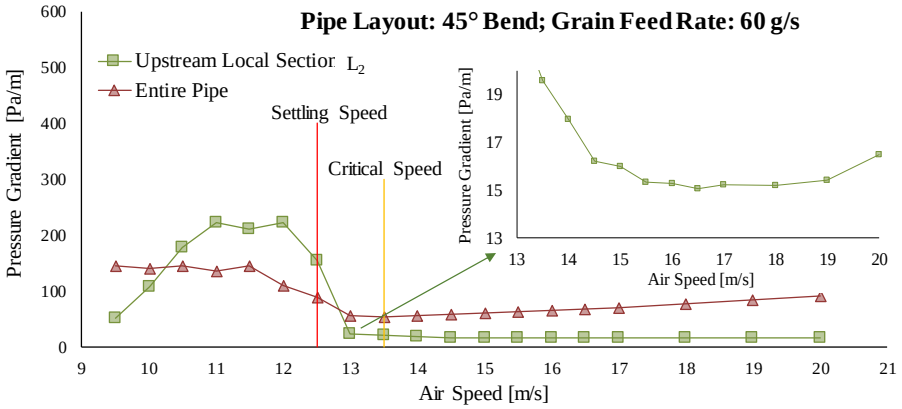

c)

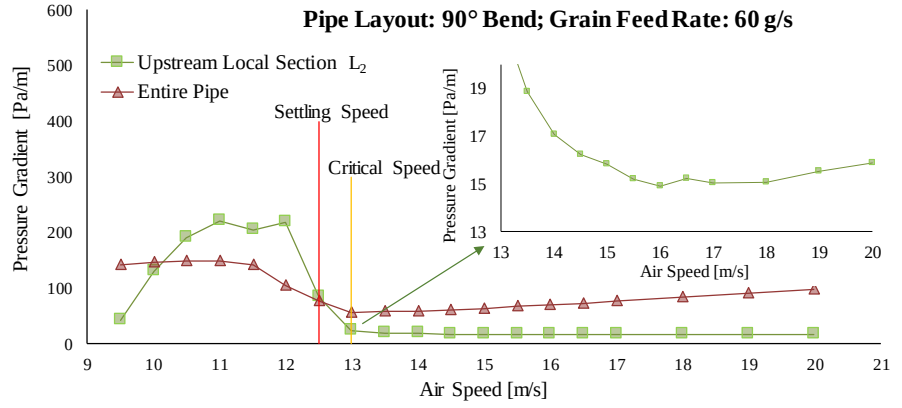

Figure 4.10: Local pressure gradient ($\Delta P_{local\text{-}L_2}$) along the section L_2, and average pressure gradient ΔP_{avg} along the whole pipe; for grain feed rate ($\dot{m}_p$) of 60 g/s and bend angles (θ) of (a) 0°, (b) 45°, and (c) 90°. Insets show the zoomed view of $\Delta P_{local\text{-}L_2}$ at $u_g \geq u_{cr}$, illustrating the increase in $\Delta P_{local\text{-}L_2}$ at higher air speed than critical speed.

At high air speeds, both $\Delta P_{local\text{-}L_2}$ and ΔP_{avg} decreased with reduction in the air speed until reaching their respective minimum values, beyond which they started to increase upon any further reduction in air speed. Also, as shown in the insets, the minima of $\Delta P_{local\text{-}L_2}$ appeared at much higher air speed than that corresponding to the minima of ΔP_{avg} (i.e. critical speed), however, the grains settled in the L_2 section only at or below the settling speed. The most likely reason for the early increase in $\Delta P_{local\text{-}L_2}$ seemed to be the change in the pipe diameter (from smaller to larger) within section L_2. It is expected that while transitioning from smaller to larger diameter pipe section, air flow in the L_2 section would have slowed down resulting in poor suspension of grains and thus increasing concentration in the lower half of the pipe. The local effect of pipe expansion was thus seen in terms of early increase in $\Delta P_{local\text{-}L_2}$ at a much higher air speed than the critical speed (u_{cr}). In other words, the local flow condition in section L_2 at higher air speed was like the flow condition in rest of the pipe at much lower air speed.

The trend of $\Delta P_{local\text{-}L_2}$ indicates that a section like L_2 (where the pipe diameter expanded) can be very useful for measuring the pressure gradient in order to proactively sense the approaching settling speed. Also, the reason for the low magnitude of $\Delta P_{local\text{-}L_2}$ seems to be the non-uniformity (expansion) in pipe diameter within section L_2. As the upstream pressure tap was mounted on the small diameter pipe and the downstream pressure tap was mounted on the large diameter pipe (Figure 4.8), the differential pressure is expected to be smaller than that in a uniform-diameter pipe: with the increase in diameter, the static pressure would also increase at the downstream pressure tap, and therefore the difference between static pressure at the upstream and the downstream pressure taps became small.

4.4.2 Bend

The bend section was made of flexible tube, which was bent (R = 0.635 m) at different angles (0.0°, 22.5°, 45.0°, 67.5°, and 90.0°) according to the test condition. The differential pressure was measured every 22.5° around the bend; therefore, the bend section for 22.5°, 45.0°, 67.5°, and 90.0° bent pipe layouts, were divided by pressure taps into one, two, three, and four subsections, respectively (Figure 4.8). For obtaining the local pressure gradient ($\Delta P_{local\text{-}bend}$) across the entire bend section, the data of pressure gradient across the respective subsections were averaged.

Due to the substantial qualitative similarities in the trend of the local pressure gradient ($\Delta P_{local\text{-}bend}$) in all of the test conditions, the discussion is presented only for a limited number of test conditions ($\dot{m}_p$ = 60 g/s and θ = 45°, and 90°) (Figure 4.11). The plotted data for the remaining test conditions are provided in Appendix B. The data of average pressure gradient (ΔP_{avg}) for the same test conditions have also been included in the plots, so that local and average trends of pressure gradient can be compared.

a)

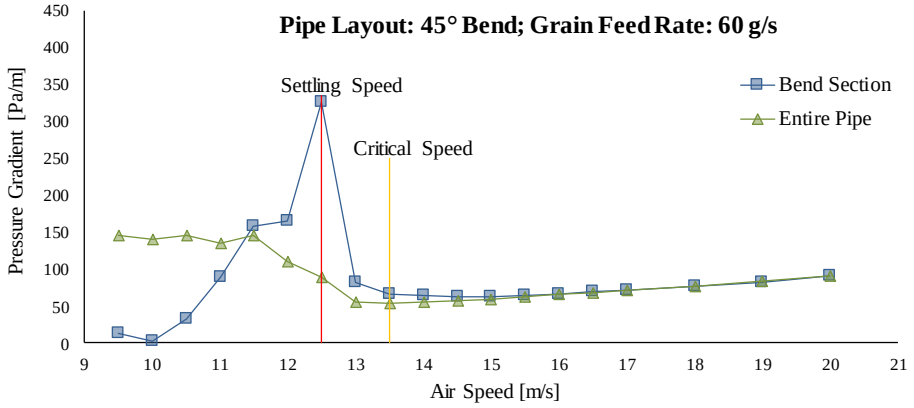

b)

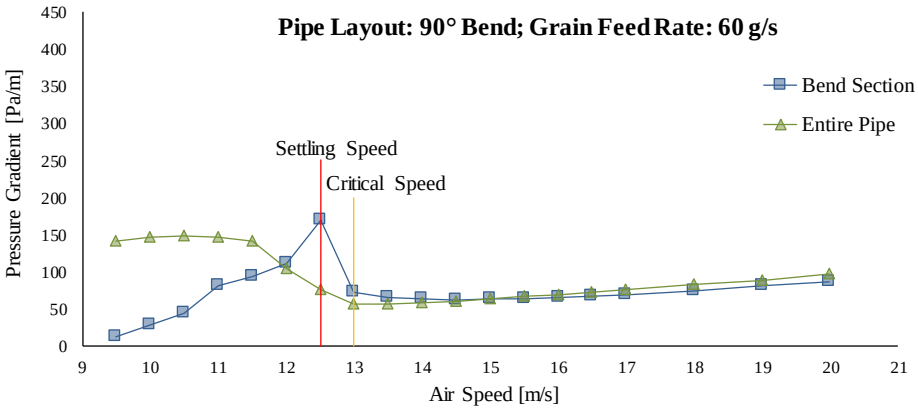

Figure 4.11: Local pressure gradient ($\Delta P_{local\text{-}bend}$) along the bend section, and average pressure gradient (ΔP_{avg}) along the entire pipe, for grain feed rate ($\dot{m}_p$) of 60 g/s, and bend angles (θ) of (a) 45.0° and (b) 90.0°.

At high air speeds, both $\Delta P_{local\text{-}bend}$ and (ΔP_{avg}) decreased with reduction in the air speed until reaching their respective minimum values, beyond which they started to increase upon any further reduction in air speed until the settling speed (u_{set}) arrived. Upon further reducing the air speed ($u_g < u_{set}$), $\Delta P_{local\text{-}bend}$ also started decreasing with a decrease in air speed. At air speeds below the settling speed, the majority of grain settling occurred at locations upstream of the bend, and less grains were reaching the bend section. Thus, at low air speeds ($u_g < u_{set}$), the pressure drop was mainly due to the frictional loss which consistently reduced with further decrease in air

speed. Therefore, at those conditions ($u_g < u_{set}$), the pressure drop as well as $\Delta P_{local\text{-}bend}$ decreased with the decrease in air speed (u_g).

However, the plots demonstrated that the minima of $\Delta P_{local\text{-}bend}$ appeared at a higher air speed than that corresponding to the minima of ΔP_{avg} (i.e. the critical speed). The most likely reason for the early increase in $\Delta P_{local\text{-}bend}$ seemed to be the higher resistance to flow in the local bend section due to the diversion of flow to an angle and the close proximity and more collisions of grains at the bend (due to the centrifugal effect). Due to the higher resistance, the flow would have slowed down, resulting in poor suspension of the grains and thus increasing the concentration in lower half of the pipe. The trend of $\Delta P_{local\text{-}bend}$ indicates that measuring the local pressure gradient along the bend section can be very useful in order to proactively identify if the operating air speed is close to the settling speed. Despite the higher resistance to flow in the bend section, there was no significant quantitative difference between $\Delta P_{local\text{-}bend}$ and ΔP_{avg}, possibly because of the large radius of bend and/or the low grain feed rate ($\dot{m}_p$).

4.4.3 Downstream of bend

The local pressure gradient $\Delta P_{local\text{-}downstream}$ was measured along approximately 11 small sections downstream of the bend. Because the reacceleration of the flow was assumed to take place immediately after the bend, only the first four downstream sections (total approximately 1.2-m-long) were considered for this discussion. For the ease of analysis, $\Delta P_{local\text{-}downstream}$ across the first four sections were averaged and were jointly designated as a single downstream section, as shown in Figure 4.8.

The trends of $\Delta P_{local\text{-}downstream}$ for selected test conditions ($\dot{m}_p$ = 20 g/s and 60 g/s; θ = 45° and 90°) are shown in Figure 4.12. The plotted data for the remaining test conditions are provided

in Appendix B. The data of average pressure gradient (ΔP_{avg}) for the same test conditions have also been included in the plots, so that local and average trends of pressure gradient can be compared.

a)

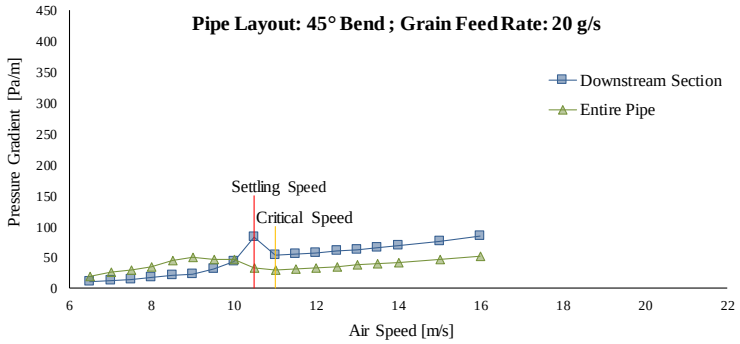

b)

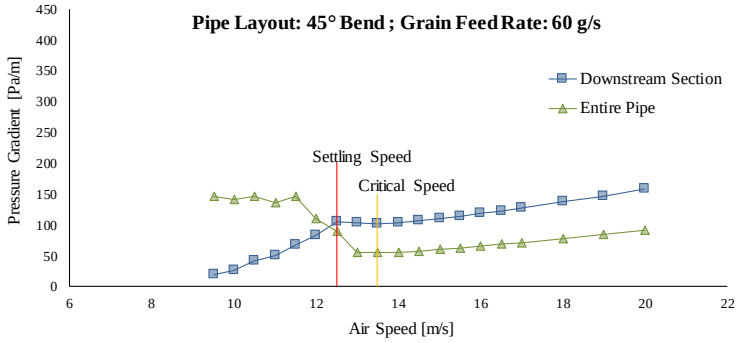

c)

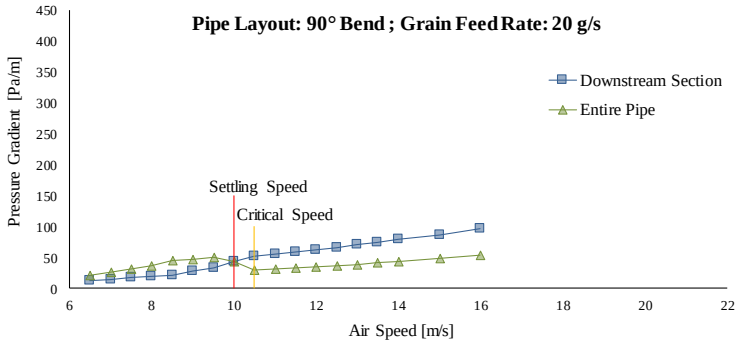

d)

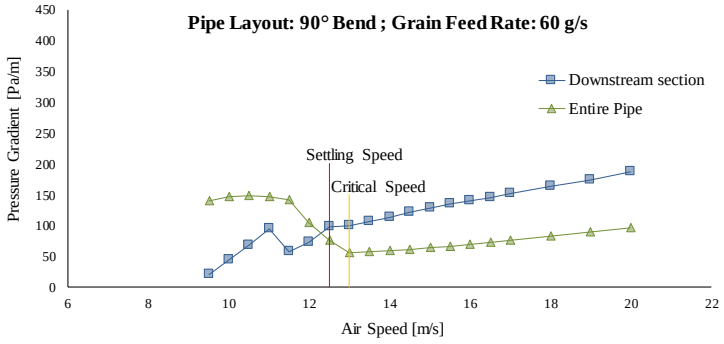

Figure 4.12: Local pressure gradient $\Delta P_{local\text{-}downstream}$ in the downstream of bend, and average pressure gradient ΔP_{avg} across the whole pipe: (a) θ = 45°, $\dot{m}_p$ = 20 g/s, (b) θ = 45°, $\dot{m}_p$ = 60 g/s, (c) θ = 90°, $\dot{m}_p$ = 20 g/s, (d) θ = 90°, $\dot{m}_p$ = 60 g/s.

The plots show that, for the most part, $\Delta P_{local\text{-}downstream}$ continuously decreased upon a decrease in the air speed. However, $\Delta P_{local\text{-}downstream}$ was sometimes also seen increasing between u_{cr} and $u_{set,}$ indicating an increase in resistance to the flow in those specific cases. At air speeds above the settling speed ($u_g > u_{set}$), the magnitude of $\Delta P_{local\text{-}downstream}$ was consistently higher than ΔP_{avg}, reflecting high pressure drop because of the flow reacceleration in bend's downstream section.

It could also be noticed that the rate of decrease in $\Delta P_{local\text{-}downstream}$ with decreasing air speed was relatively higher at air speeds below the settling speed ($u_g < u_{set}$). This probably happened because, upon going below the settling speed, the grains started settling mainly in the bend and its upstream sections. Moreover, the number of settling grains increased with further reduction in air speed. As a result, the number of grains flowing through the bend's downstream section rapidly decreased with every further reduction in air speed because of the upstream settling. Thus, due to the lesser number of grains flowing through the bend's downstream section, the local resistance to air flow due to the grains decreased at every next lower air speed, which was indicated by the rapid reduction in the local pressure gradient $\Delta P_{local\text{-}downstream}$. Hence, the trend of decrease in $\Delta P_{local\text{-}downstream}$ could indicate the corresponding flow condition: higher reduction rate indicating the settling at upstream and lower rate indicating the flow with no settling of grains.

4.5 Variation in pressure gradient along the pipe and its utility in identifying the location of settling of grains

In Section 4.3, the data demonstrated that an increase in the pressure gradient on reducing the air speed was an indication of the poor suspension of grains and of the operating air speed being close to the settling speed. It also showed that the trend of average pressure gradient could help in predicting the optimum air speed for the conveying process. Though the characteristics of

the average pressure gradient were promising, and its measurement required only one pressure transmitter across the entire pipe, it did not help in identifying the location of grains settling, which could be a crucial requirement for troubleshooting long conveying lines.

This section presents a discussion on the possibility of identifying the location of grains settling in the pipe with the help of local differential pressure measurements along small sections of the pipe. For the purpose of this analysis, the local pressure gradient data (during the grains transportation) were normalized by their respective air only flow data. The normalization assisted in amplifying the change in pressure gradient during the conveying process. The data for this particular analysis were taken only from one trial of each test, instead of the average of three trials. This was done because the locations of settling were not necessarily exactly similar in all three repetitions of the tests, and the data from a single test would provide a more accurate correlation between the grains settling and the resulting pressure gradient.

The data were plotted as normalized-local pressure gradient vs. pipe length, and four air speeds (settling speed and three higher air speeds) have been considered in the plots. To highlight the change in pressure gradient in the case of grains settling, the respective data points are demonstrated by large circular markers.

The focus of this study was to analyze the settling conditions, and prior to conducting the tests, it was assumed that the settling would most likely happen in the bend and downstream of bend. Therefore, the pressure data collection was also focussed around the bend region (including downstream). Out of 14 local sections along the pipe in which pressure drop was measured, one was 0.5 m downstream of the feeding point and the remaining 13 were in continuous series beginning from 6.05 m downstream of the feeding point to the exit of pipe.

4.5.1 Straight pipe

The local pressure gradient was measured across 14 local sections along the straight pipe, as shown in Figure 4.8. The variation in local pressure gradient along the straight pipe at four different air speeds (close to the settling speed) is shown in Figure 4.13. The plots show that in the case of grains settling in the pipe (at the settling speed), the normalized-local pressure gradient ($\Delta P_{normalized\text{-}local}$) fluctuated and increased sharply. Also, the highest peaks were obtained at locations where the majority of the grains settled down, indicating the significant effect of stationary grains on the pressure drop.

(a)

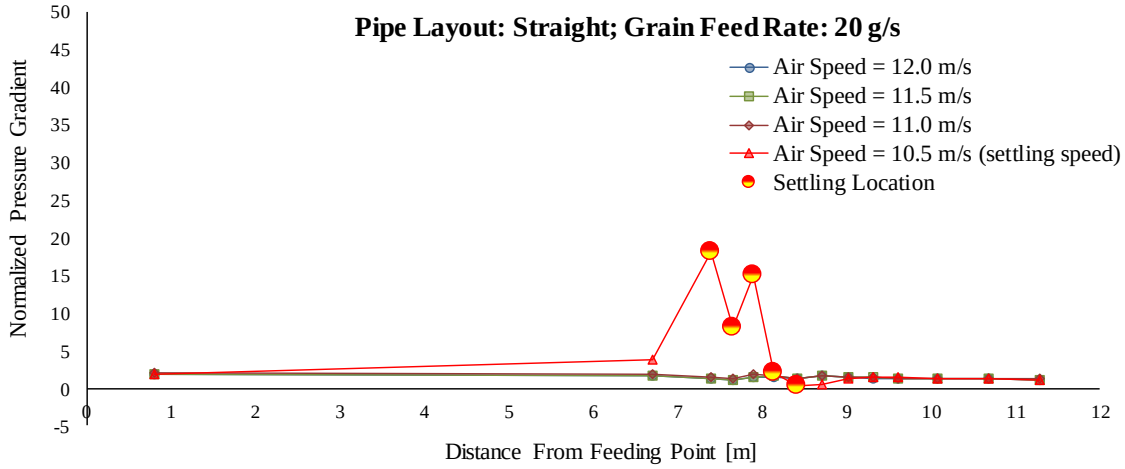

(b)

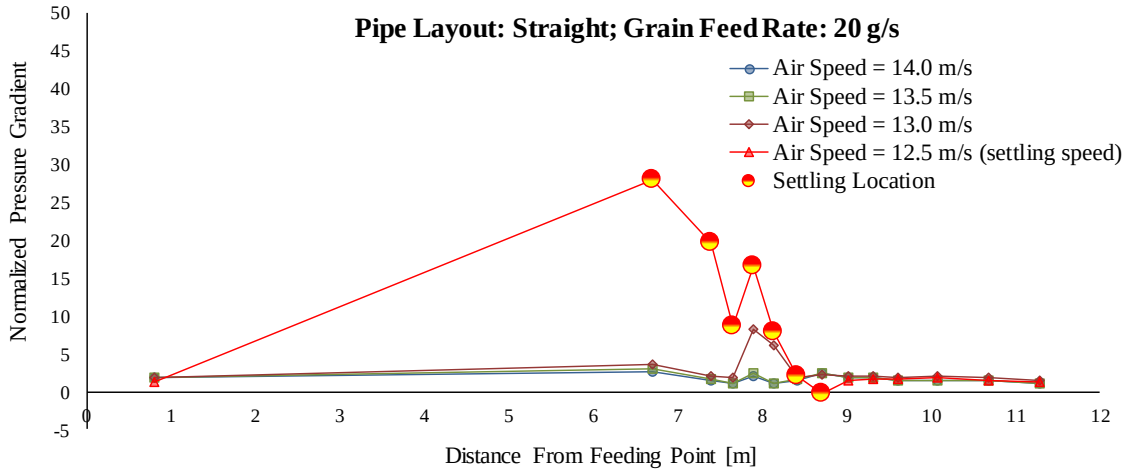

(c)

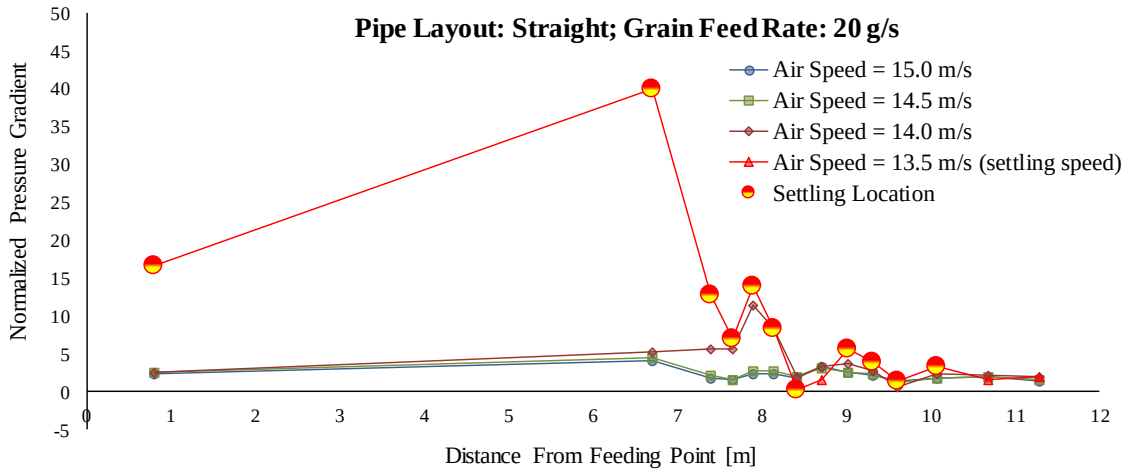

Figure 4.13: Normalized-local pressure gradient ($\Delta P_{normalized\text{-}local}$) along the straight pipe for grain feed rates ($\dot{m}_p$) of (a) 20 g/s (b) 60 g/s (c) 100 g/s.

For low grain feed rate ($\dot{m}_p$ = 20 g/s), the curves were found to overlap at high air speeds ($u_g > u_{set}$). However, at the settling speed when the grains settled in the pipe, $\Delta P_{normalized\text{-}local}$

substantially fluctuated and reached the peak values. It indicated that the contribution of the grain flow to the pressure drop remained almost constant at air speeds above the settling speed, but fluctuated at the settling speed due to high instability in the flow. For a higher grain feed rate (60 g/s and 100 g/s), the peaks in $\Delta P_{normalized\text{-}local}$ were obtained not only at the settling speed, but also at the air speeds just above the settling speed, indicating that the resistance to air flow due to the grains started increasing at air speeds right above the settling speed. Similar trends were also seen in Section 4.3 where the pressure gradient for $\dot{m}_p$ = 20 g/s showed a sudden increase right at the settling speed, whereas, for higher solid feed rates, the pressure gradient started increasing at air speeds slightly above the settling speed.

The sharp fluctuation in $\Delta P_{normalized\text{-}local}$ was not the same at all locations where the grains settled down, yet the fluctuations and increments were conveniently identifiable at the locations where substantial settling of grains occurred. It could also be noticed that $\Delta P_{normalized\text{-}local}$ was not constant along the pipe even at high air speeds when there was no settling of grains. One of the likely reasons for a slightly inconsistent trend of $\Delta P_{normalized\text{-}local}$ in downstream sections upon grains settling could be the flexible tube section, which was used in the middle of the pipe for creating the bend, had a larger cross sectional area than the rest of the pipe. The transition of flow from small to large and then large to small cross-section of pipe might have possibly resulted in the non-uniformity in flow along the pipe. Another reason for the same was possibly the small size of the local sections, as in small local sections there was high probability that the flow conditions were randomly changing within the section with very small pressure drop. In this condition, perhaps the sensors with higher resolution might have been more suitable. Thus, the results suggested that if the pipe was uniform throughout and the local pipe sections were longer, the detection of settling-locations downstream might have been even more effective.

4.5.2 Bent pipe

The local pressure gradient was measured across 14 local sections along the bent pipe as shown in Figure 4.8. The variations in local pressure gradient along the bent pipe (θ = 90°) at four different air speeds (close to the settling speed) are shown by the plots in Figure 4.14 (for θ = 90°); for the remaining test conditions, the plots are provided in Appendix B. For the respective grain feed rates and air speeds, the trends of $\Delta P_{normalized\text{-}local}$ were substantially similar along the pipe.

(a)

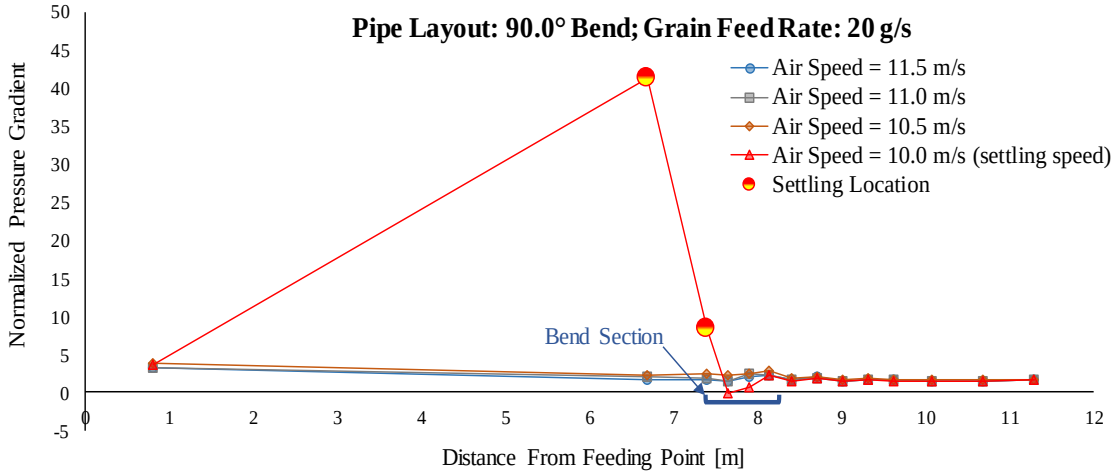

(b)

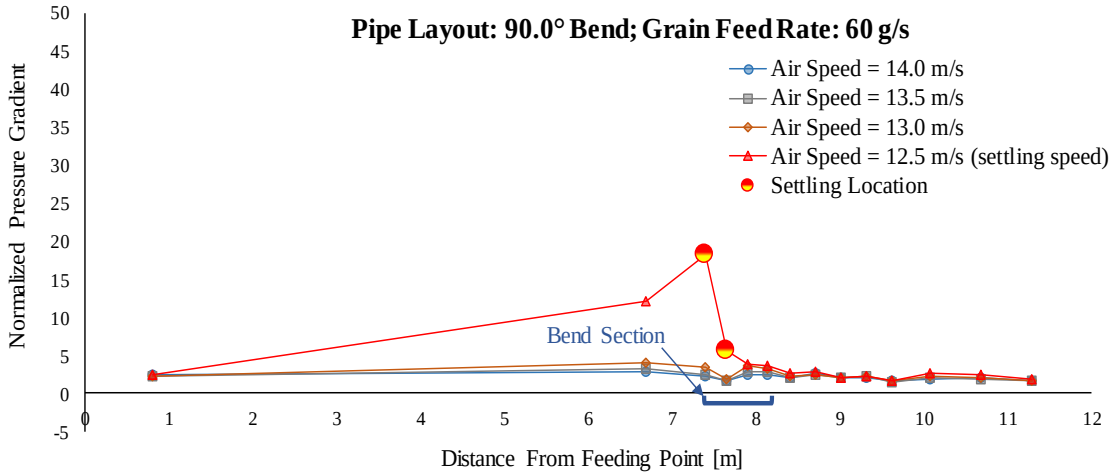

(c)

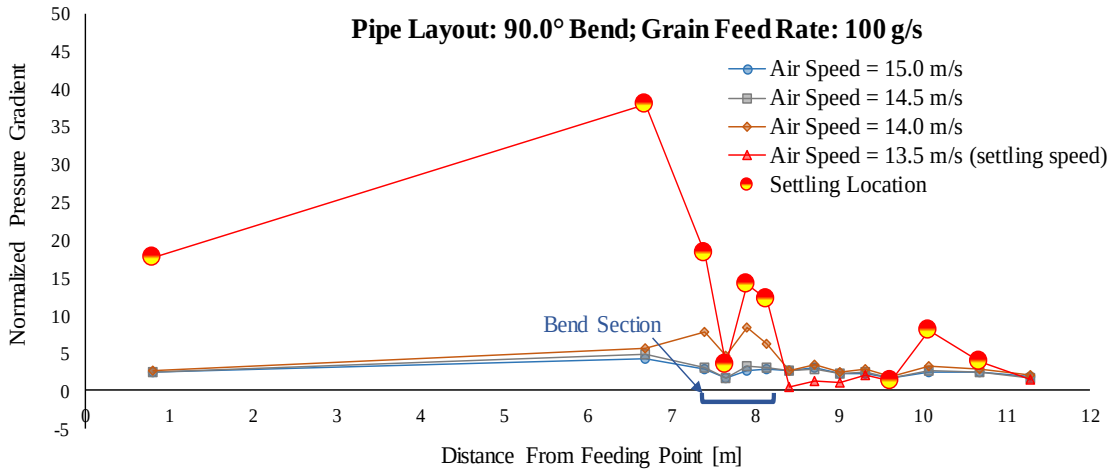

Figure 4.14: Normalized-local pressure gradient $\Delta P_{normalized\text{-}local}$ along the bent pipe with 90.0° bend angle, for grain feed rates ($\dot{m}_p$) of (a) 20 g/s (b) 60 g/s (c) 100 g/s. Settling location is where the grains settled down in pipe at settling speed.

Given the consistency in the trends of $\Delta P_{normalized\text{-}local}$ along the straight as well as bent pipe, this methodology seems an easy but highly reliable methodology for identifying any settling in the pipe. Moreover, in the locations where the settling of grains was intense, the fluctuations in $\Delta P_{normalized\text{-}local}$ were clearly identifiable. Moreover, if the local pipe sections were a little longer, the settling could have been identified more effectively in those pipe sections where the settling was quite mild.

Chapter 5 : Conclusions and Future Work

5.1 Conclusions

This study examined the feasibility of using the pressure drop data to identify the flow conditions (pre-settling and settling) in the pneumatic conveying of wheat grains through a horizontal conveying line. The tests were conducted for five different pipe layouts in a horizontal plane with the bend angles of 0.0°, 22.5°, 45.0°, 67.5°, and 90.0°, and three solid feed rates of 20 g/s, 60 g/s, and 100 g/s. The data (pressure drop) were collected for a range of air speeds (6.5 m/s - 21.0 m/s) so that a wide spectrum of flow conditions could be observed. The data were analyzed by plotting them as pressure drop per unit length of section (pressure gradient) vs. air speed.

The inclusion of a bend (between 0°-90° angle) in the conveying line did not seem to affect the overall flow conditions and the pressure drop. The initial hypothesis for these tests was that the bend angle should result in significantly increased pressure drop and/or settling speed, however, the increase in pressure drop was only minimal, and the settling speed was found to remain largely unchanged despite any change in the bend angle (except for the 20 g/s and 90° case). It is speculated that the fan controller (which consistently maintained the target air speed during the test) did not let the flow slow down in the bend and thus played an important role in keeping the settling speed unchanged across all tested pipe layouts. It indicated the usefulness of the fan controller for reducing the probability of settling. Also, the large bend radius (0.64 m, ~20x pipe diameter) might have diluted the overall bend effect.

The data analysis demonstrated that the pressure gradient trend could very effectively be used to identify the corresponding flow conditions, and it could also suggest the optimum air speed for the process. The average pressure gradient (in the entire length of pipe) consistently followed

a qualitative trend with change in air speed for all tested pipe layouts and solid feed rates. In all tests, the average pressure gradient showed a detectable transition at an air speed (critical speed) slightly higher (by 0.5 - 1.5 m/s) than the settling speed (air speed at which the grains started settling down in the pipe). The air speed corresponding to this transition of pressure gradient trend was termed the critical speed. The average pressure gradient at the critical speed was at its minimum, whereas upon going above or below the critical speed, the pressure gradient monotonically increased. As the critical speed was consistently higher than the settling speed by a small yet detectable difference (0.5 - 1.5 m/s), and the corresponding average pressure gradient was at its minimum, the critical speed could be recommended as the optimum air speed for any of the tested solid feed rates and pipe layouts. Upon an increase in the grain feed rate, the settling speed increased, however the increase in settling speed was much smaller relative to the increase in grain feed rate. This illustrated that the load carrying capacity of air also improved with an increase in solids feed rate, which would be helpful in optimizing the transportation rate in a conveying process.

The trend of local pressure gradient was found to be dependent on the grain settling locations and the pipe's local configuration. The local pressure gradient was not affected by the grain settling at its downstream, and could not indicate the occurrence of settling in the pipe. The qualitative trend of local pressure gradient in upstream of the bend and in the bend was quite similar to average pressure gradient in the entire pipe, however the minimum pressure drop upstream of the bend and in the bend section appeared at a higher air speed than that in the entire pipe. The qualitative trend of local pressure gradient in the bend's downstream section was different from the average pressure gradient because in the case of grain settling very few grains moved past the bend section and therefore the pressure drop decreased at every next lower air

speed. The observations indicated that the location of the local pressure drop measurement seemed to play an important role in deciding their effectiveness in accurately identifying the overall flow condition.

The pipe section that was used to introduce a bend in the conveying line happened to be larger in cross sectional area than the rest of the pipe (by 11.4%). Since irrespective of the pipe layout (straight or bent) and bend angle (0° - 90°), the grains were found to settle mostly in this particular pipe section (a small pipe section of slightly larger diameter), it was speculated that this kind of expansion in the pipe perhaps could be used to constrain the location of grain settling in the pipe. This characteristic could especially be useful in easier monitoring of the flow condition by creating a dedicated observation section and cleaning window (if needed).

The trend of normalized local pressure drop (normalized by the corresponding local pressure drop in air only flow) demonstrated that by measuring the pressure drop at regular intervals along the pipe, the location of grain settling can effectively be identified within 60 s of its occurrence. This feature could be very useful particularly for a long pipeline also having a complex layout.

5.2 Future work and recommendations

The study successfully demonstrated the applicability of the trend of pressure gradient for the pneumatic conveying of wheat grains, however, there are few remaining unanswered questions which require further investigation.

As the data for each test condition were collected separately in a new experiment, its (data) applicability to understand and model the flow transition from non-settling to settling like conditions is limited. It is recommended that the future studies also collect the continuous data (of

total 180 s) while transitioning from normal flow to the grains settling. Such data could be highly valuable for developing a control algorithm for pneumatic conveying processes.

Furthermore, because the data collection was initiated after stabilizing the air-grain flow for 60 s, it did not provide an insight on initial flow development. It is recommended that future studies include this investigation in case the initial flow development can provide any early signs of settling behaviour.

Experiments with smaller bend radii are recommended to expand the understanding of bend effect on the pneumatic conveying of wheat grains.

References

Akilli, H., Levy, E. K. & Sahin, B., 2005. Investigation of gas-solid flow structure after a 90 degree vertical-to-horizontal elbow for low conveying gas velocities. *Advanced Powder Technology,* 16(3), pp. 261-274.

Albion, K., Briens, L., Briens, C. & Berutti, F., 2007. Flow regime determination in horizontal pneumatic transport of fine powders using non-intrusive acoustic probes. *Powder Technology,* 172(3), pp. 157-166.

Barbosa, P. R., Crivelaro, K. C. O. & Seleghim Jr, P., 2010. On the application of self-organizing neural networks in gas-liquid and gas-solid flow regime identification. *Journal of the Brazilian Society of Mechanical Sciences and Engineering,* 32(1), pp. 15-20.

Barbosa, P. R. & Seleghim Jr., P., 2003. Improving the power consumption inpneumatic conveying sytems by adaptive control of the flow regime. *Journal of the Brazilian Society of Mechanical Sciences and Engineering,* 25(4), pp. 373-377.

Cabrejos, F. J. & Klinzing, G. E., 1995. Characterization of dilute gas-solids flow using the rescaled range analysis. *Powder Technology,* 84(1), pp. 139-156.

Dhodapkar, S., Solt, P. & Klinzing, G., 2009. Understanding bends in pneumatic conveying systems. *Chemical Engineering,* April, pp. 53-60.

Dhole, L. P., Bhuyar, L. B. & Awari, G. K., 2011. Application of dilute phase pull push type pneumatic conveying system for conveying of powdered and granular material. *Journal of Engineering Research and Studies,* 2(4), pp. 247-251.

Fraige, F. Y. & Langston, P. A., 2006. Horizontal pneumatic conveying: a 3D distinct element model. *Granular Matter,* 8(1), pp. 67-80.

Geldart, D., 1973. Types of gas fluidization. *Powder Technology,* 7(1), pp. 285-292.

Gelinske, J. N., Reich, A. A. & Batcheller, B. D., 2015. *Air Seeder Monitoring and Equalization System Using Acoustic Sensors.* United States, Patent No. 8950260 B2.

Goering, K. J., Ferree, P. E. & Dzubak, A. L., 2007. *Conveying Duct Pressure Monitor System for Controlling Harvester Speed.* United States, Patent No. 7249449 B2.

Gomes, L. M. & Mesquita, A. L. A., 2014. On the prediction of pickup and saltation velocities in Pneumatic Conveying. *Brazilian Journal of Chemical Engineering,* 31(1), pp. 35-46.

Guner, M., 2007. Pneumatic conveying characteristics of some agricultural seeds. *Journal of Food Engineering,* 80(1), pp. 904-913.

Gupta, P. K. & Pagalthivarthi, K. V., 2006. A comparative study of the effect of model lift coefficients on particle trajectory. *Indian Journal of Engineering & Material Sciences,* 13(1), pp. 293-306.

Hapman, S. G., 2005. Choosing a pneumatic conveying system: Pressure or vacuum, dense or dilute phase?. *Powder and Bulk Engineering,* 19(3), pp. 31-33.

Herbreteau, C. & Bouard, R., 2000. Experimental study of parameters which influence the energy minimum in horizontal gas-solid conveying. *Powder Technology,* 112(1), pp. 213-220.

Hong, J., Shen, Y. & Tomita, Y., 1995. Phase diagrams in dense phase pneumatic transport. *Powder Technology,* 84(1), pp. 213-219.

ISO 5167-4, 2003. Measurement of fluid flow by means of pressure differential devices inserted in circular cross-section conduits running full - Part 4: Venturi tubes. *International Organization for Standardization.*

Jama, G. A., Klinzing, G. E. & Rizk, F., 2000. An investigation of the prevailing flow patterns and pressure fluctuation near the presure minimum and unstable conveying zone of pneumatic transport systems. *Powder Technology,* 112(1), pp. 87-93.

Kai, X., Xiaolei, G., Xingliang, C. & Kai, L., 2013. Minimum pressure drop velocity and stability analysis in pneumatic conveying of pulverized coal in commercial-scale horizontal pipe. *Chemical Industry and Engineering Society of China,* 64(6), pp. 1969-1975.

Klinzing, G. E., Rizk, F., Marcus, R. & Leung, L. S., 2010. *Pneumatic Conveying of Solids.* New York: Springer Science+Business Media B. V..

Konrad, K., 1986. Dense-phase pneumatic conveying: A review. *Powder Technology,* 49(1), pp. 1-35.

Matsumoto, S. & Saito, S., 1970. On the mechanism of suspension of particles in horizontal pneumatic conveyimg: Monte Carlo simulation based on the irregular bouncing model. *Journal of Chemical Engineering of Japan,* 3(1), pp. 83-92.

Michaelids, E. E. & Lai, F. C., 1987. Pressure loss through return bends in air-solid flows. *International Journal of Multiphase Flow,* 13(2), pp. 269-274.

Mills, D., 2004. *Pneumatic Conveying Design Guide.* Burlington: Elsevier Butterworth-Heinemann.

Molerus, O. & Burschka, A., 1995. Pneumatic transport of cross-grained materials. *Chemical Engineering and Processing,* 34(1), pp. 173-184.

Rabinovich, E. & Kalman, H., 2011. Threshold velocities of particle-fluid flows in horizontal pipes and ducts: literature review. *Reviews in Chemical Engineering,* 27(1), pp. 215-239.

Rinoshika, A., 2014. Dilute pneumatic conveying of a horizontal curved 90 degree bend with soft fins or dune model. *Powder Technology,* 254(1), pp. 291-298.

Santos, S. M. et al., 2011. Dilute phase pneumatic conveying of polystyrene particles: Pressure drop curve and particles distribution over the pipe cross-section. *Brazilian Journal of Chemical Engineering,* 28(1), pp. 81-88.

Smith, D., 2008. *System and Method for Detecting a Condition Indicative of Plugging of a Discharge Path of an Agricultural Combine.* United States, Patent No. 7381130 B2.

Tevs, N. R., Bethune, E. M. & Dragne, R. N., 2003. *Tube Blockage Monitor.* United States, Patent No. 6661514.

Tevs, N. R., Bethune, E. M. & Dragne, R. N., 2003. *Tube Blockage Monitor.* United States, Patent No. 6661514.

Thomas, D. G., 1962. Transport characteristics of suspensions: Part VI. Minimum transport velocity for large particle size suspensions in round horizontal pipes. *American Institute of Chemical Engineers,* 8(3), pp. 373-378.

Thomas, J. C. et al., 1998. *Air Seeder Blockage Monitoring System.* United States, Patent No. 5831542.

Tsilingiris, P. T., 2008. Thermophysical and transport properties of humid air at temperature range between 0 and 100 deg C. *Energy Conversion and Management,* 49(1), pp. 1098-1110.

Tsuji, Y. & Morikawa, Y., 1982. Flow pattern and pressure fluctuation in air-solid two-phase flow in a pipe at low air velocities. *International Journal of Multiphase Flow,* 8(4), pp. 329-341.

Zenz, F. A., 1949. Two-phase fluid-solid flow. *Industrial and Engineering Chemistry,* 41(12), pp. 2801-2806.

Appendix A: Variables (z_v, f (P,T), *and* P_{sv}) for Air Density (ρ) Equation

(i) Saturated vapor pressure P_{sv} (in kPa)

Tsilingiris (2008) determined the value of P_{sv} from a polynomial expression (Equation A.1), which was obtained by fitting the P_{sv} data (as per the thermodynamic properties of water) between 0 °C to 100 °C temperature. E_0, E_1, E_2, E_3, *and* E_4 are the constants in Equation A.1.

$$P_{sv} = E_0 + E_1 t + E_2 t^2 + E_3 t^3 + E_4 t^4 \quad \textbf{Equation A.1}$$

where,

t = Temperature inside the venturi (°C),

E_0 = 0.7073034146,

E_1 = -2.703615165 X 10^{-2},

E_2 = 4.36088211 X 10^{-3},

E_3 = -4.662575642 X 10^{-5}, and

E_4 = 1.034693708 X 10^{-6}.

(ii) Compressibility factor z_v

$$z_v = 1 + A\ P_{sv} + B\ P_{sv}^2 \quad \textbf{Equation A.2}$$

$$A = C_1 + C_2\ e^{\frac{c_3}{T}} \quad \textbf{Equation A.3}$$

$$B = K_1 + K_2\ e^{\frac{K_3}{T}} \quad \textbf{Equation A.4}$$

where,

C_1 = 0.7 X 10^{-8} Pa^{-1},

C_2 = -0.147184 X 10^{-8} Pa^{-1},

C_3 = 1734.29 K^{-1},

K_1 = -0.104 X 10^{-14} Pa^{-2},

K_2 = 0.335297 X 10^{-17} Pa^{-2}, and

K_3 = 3645.09 K^{-1}.

(ii) Enhancement factor f (*P,T*)

Tsilingiris (2008) calculated the f(*P,T*) by a simplified fitting expression (Equation A.5). $A_0, A_1, A_2, A_3, B_0, B_1, B_2, and\ B_3$ are the constants in Equation A.6 and Equation A.7.

$$f(P,T) = \exp\left[\xi_1 \left(1 - \frac{P_{sv}}{P_0}\right) + \xi_2 \left(\frac{P_{sv}}{P_0} - 1\right)\right] \quad \textbf{Equation A.5}$$

$$\xi_1 = \sum_{i=0}^{3} A_i\ T^i \quad \textbf{Equation A.6}$$

$$\xi_2 = exp\left[\sum_{i=0}^{3} B_i\ T^i\right] \quad \textbf{Equation A.7}$$

where,

T = Temperature inside the venturi (K),

A_0 = 3.53624 X 10^{-4} ,

A_1 = 2.93228 X 10^{-5} ,

A_2 = 2.61474 X 10^{-7} ,

A_3 = 8.57538 X 10^{-9} ,

B_0 = -1.07588 X 10,$^{-1}$

B_1 = 6.32529 X 10,$^{-2}$

B_2 = -2.53591 X 10,$^{-4}$ and

B_3 = 6.33784 X 10^{-7} .

Appendix B: Additional Plots for Chapter 4 (Results and Discussion)

Upstream of the bend – Section L_1

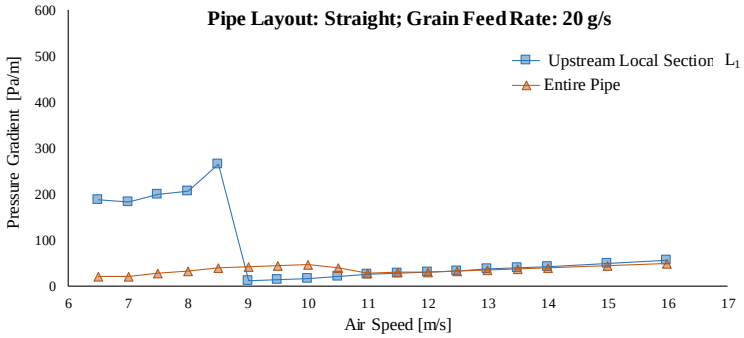

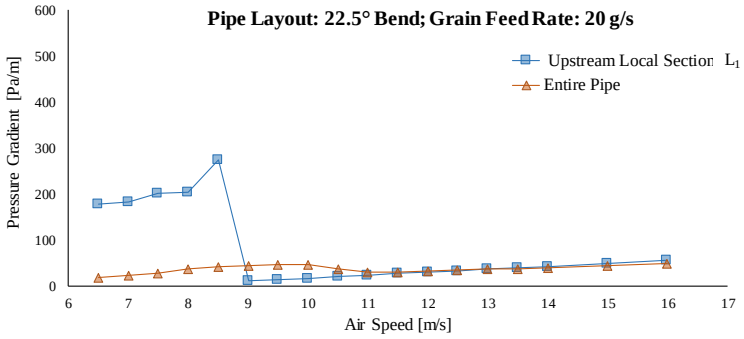

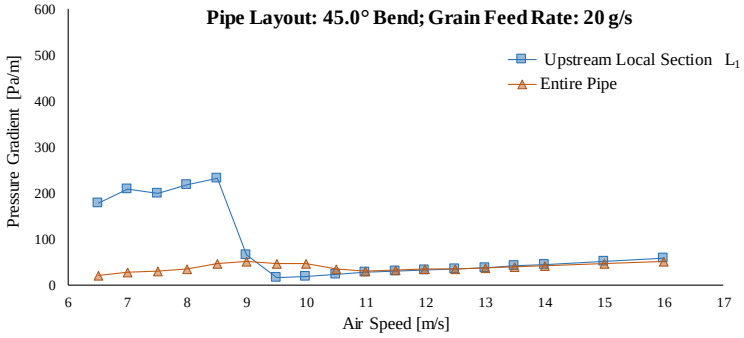

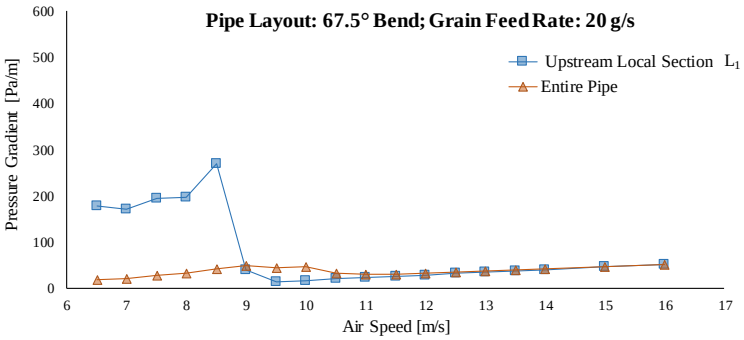

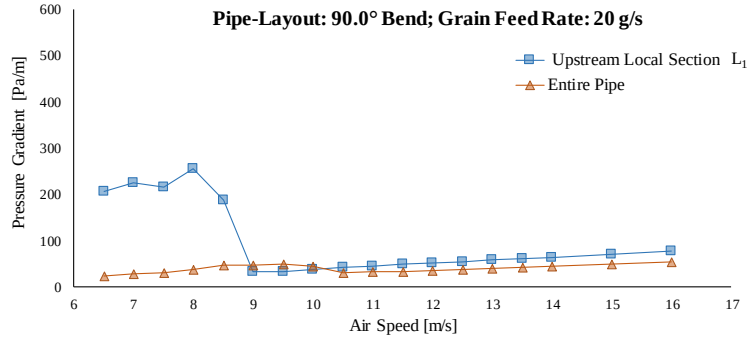
Pipe-Layout: 90.0° Bend; Grain Feed Rate: 20 g/s
Upstream Local Section L1
Entire Pipe
Pressure Gradient [Pa/m]
Air Speed [m/s]

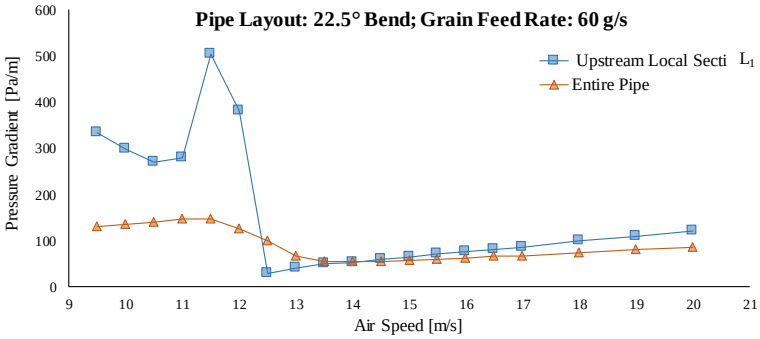
Pipe Layout: 22.5° Bend; Grain Feed Rate: 60 g/s
Upstream Local Secti L1
Entire Pipe
Pressure Gradient [Pa/m]
Air Speed [m/s]

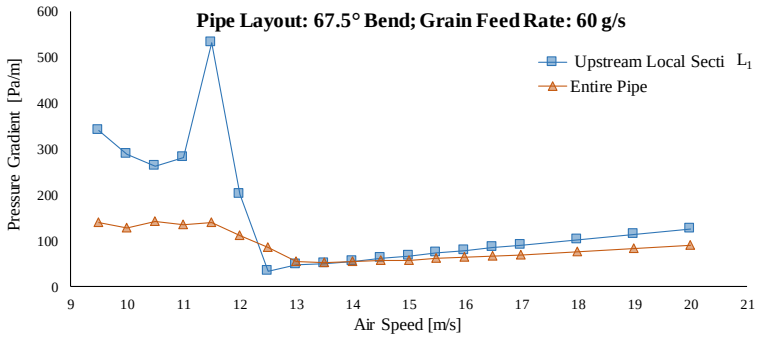
Pipe Layout: 67.5° Bend; Grain Feed Rate: 60 g/s
Upstream Local Secti L1
Entire Pipe
Pressure Gradient [Pa/m]
Air Speed [m/s]

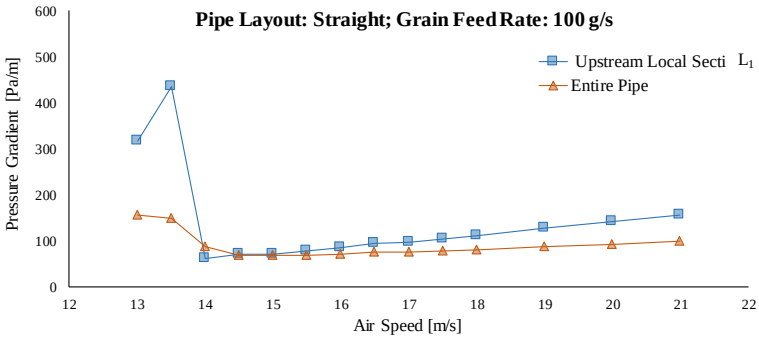
Pipe Layout: Straight; Grain Feed Rate: 100 g/s
Upstream Local Secti L1
Entire Pipe
Pressure Gradient [Pa/m]
Air Speed [m/s]

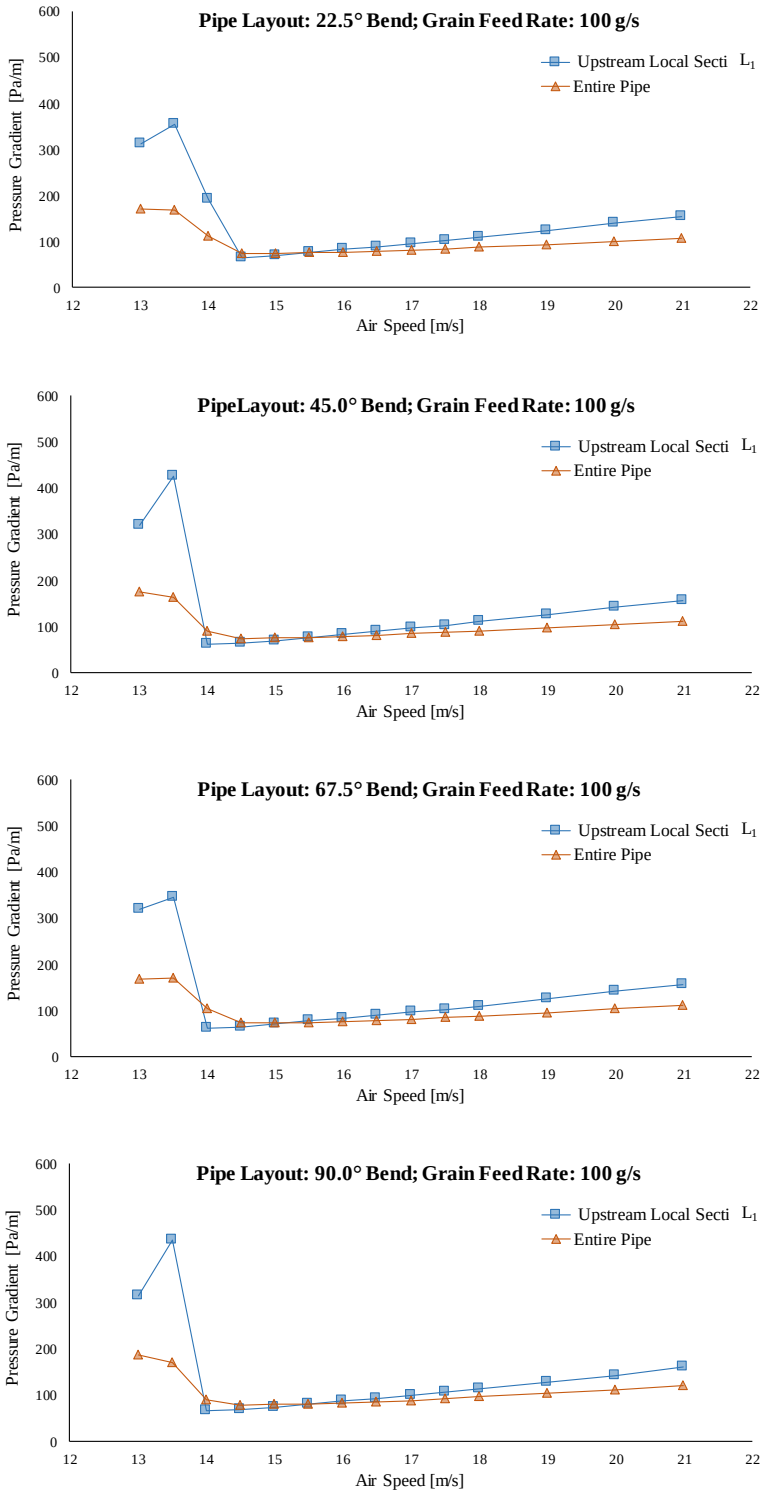

Figure B.1: Trend of local pressure gradient in section L_1 vs. average pressure gradient in entire pipe. Respective pipe layout and grain feed rate are given in the chart title.

Upstream of the bend – Section L2

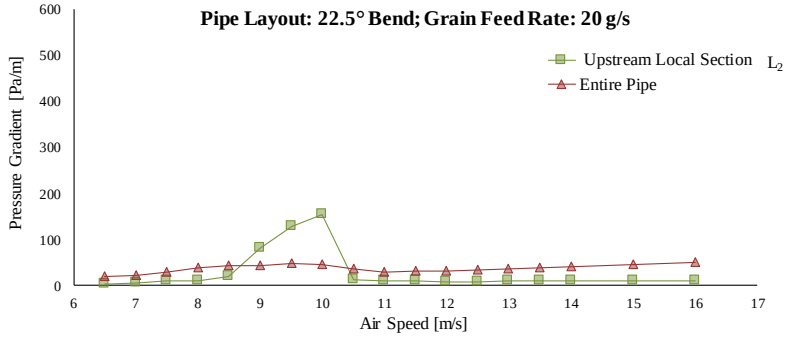

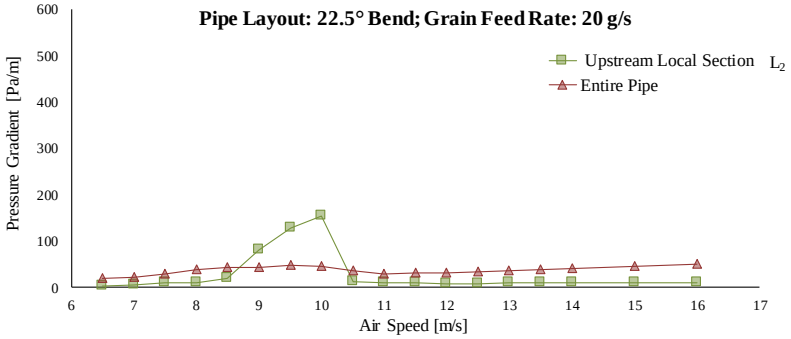

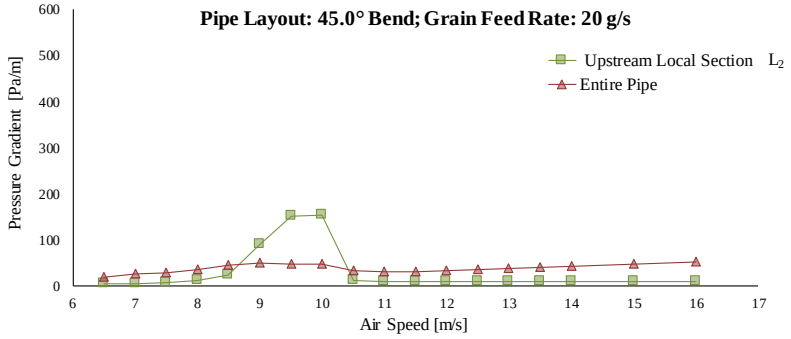

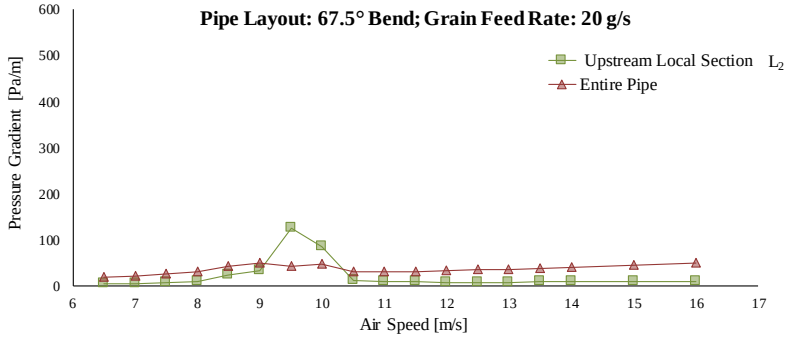

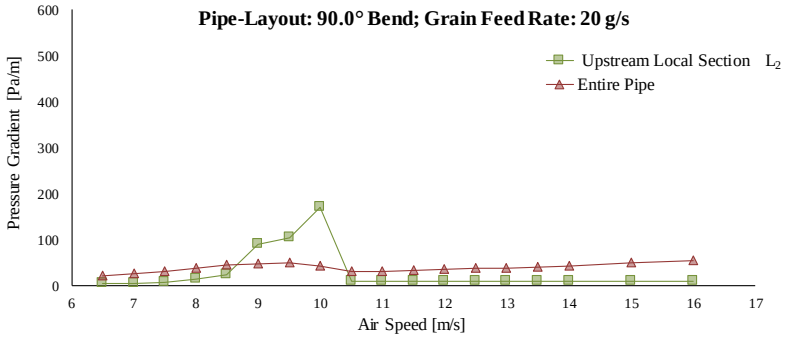
Pipe-Layout: 90.0° Bend; Grain Feed Rate: 20 g/s
Upstream Local Section L2
Entire Pipe
Pressure Gradient [Pa/m]
Air Speed [m/s]

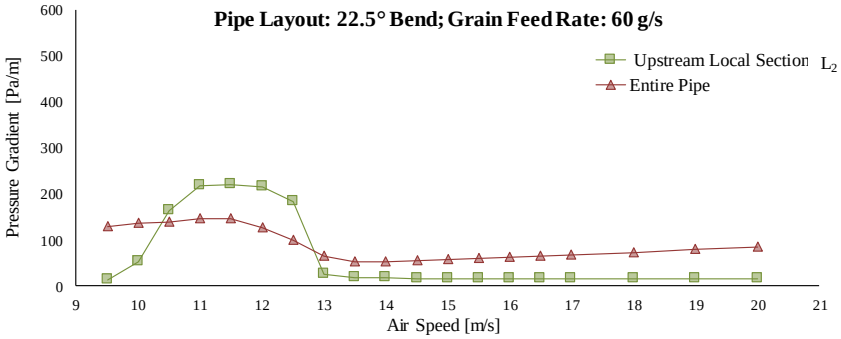
Pipe Layout: 22.5° Bend; Grain Feed Rate: 60 g/s
Upstream Local Section L2
Entire Pipe
Pressure Gradient [Pa/m]
Air Speed [m/s]

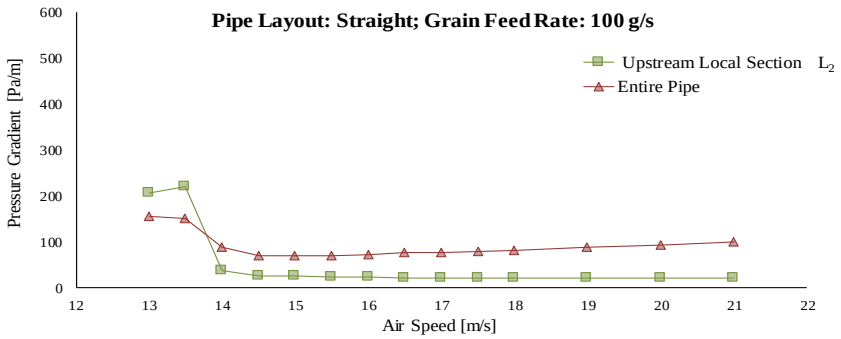
Pipe Layout: Straight; Grain Feed Rate: 100 g/s
Upstream Local Section L2
Entire Pipe
Pressure Gradient [Pa/m]
Air Speed [m/s]

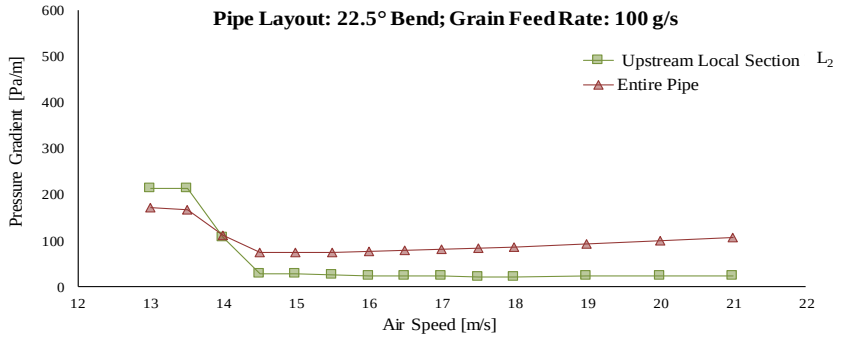
Pipe Layout: 22.5° Bend; Grain Feed Rate: 100 g/s
Upstream Local Section L2
Entire Pipe
Pressure Gradient [Pa/m]
Air Speed [m/s]

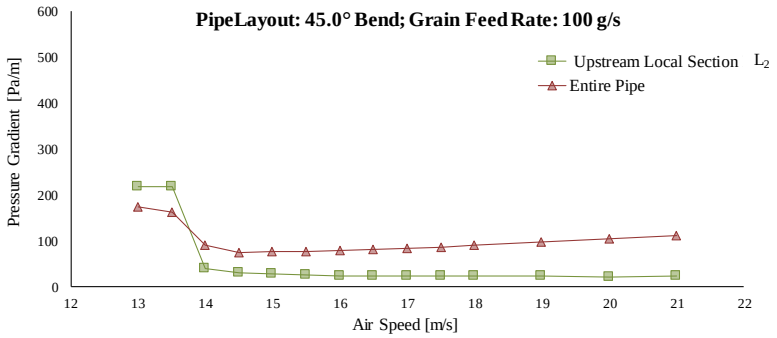

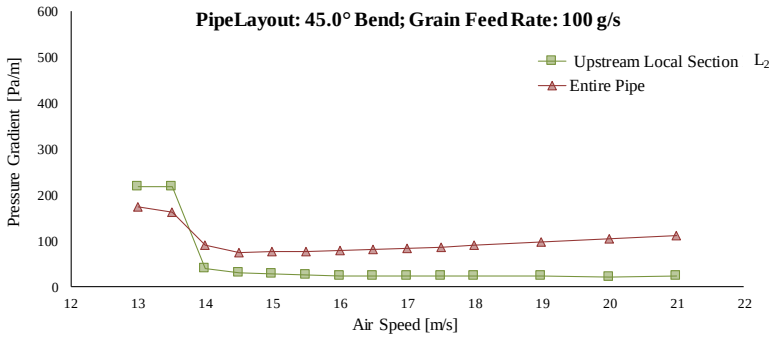

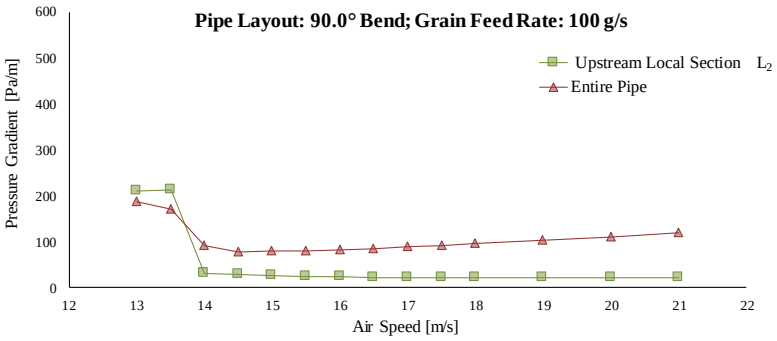

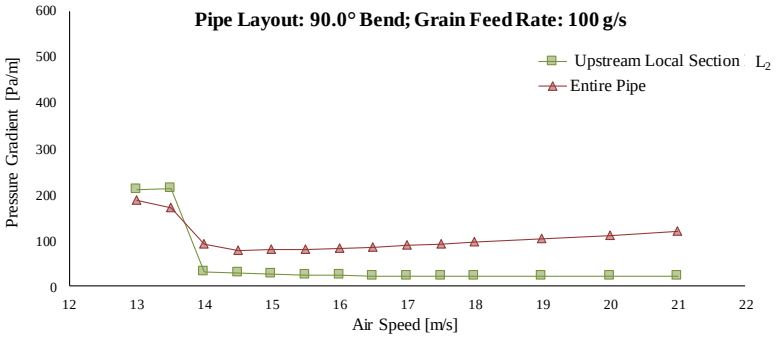

Figure B.2: Trend of local pressure gradient in section L_2 vs. average pressure gradient in entire pipe. Respective pipe layout and grain feed rate are given in the chart title.

Bend Section

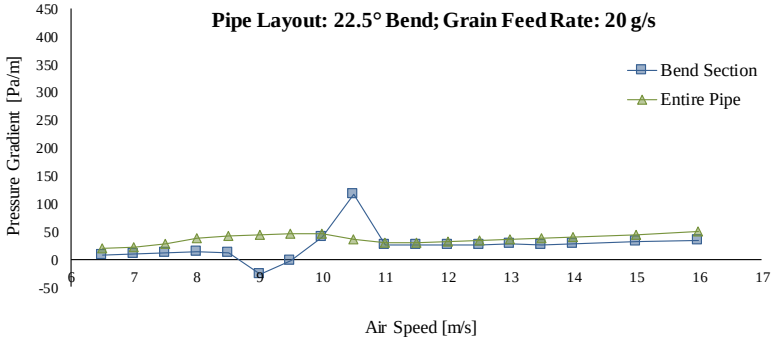

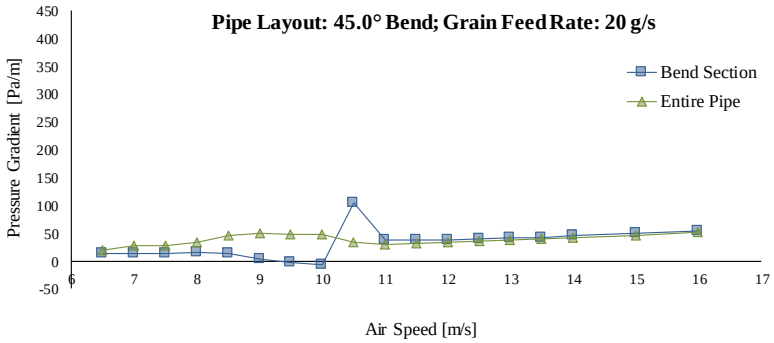

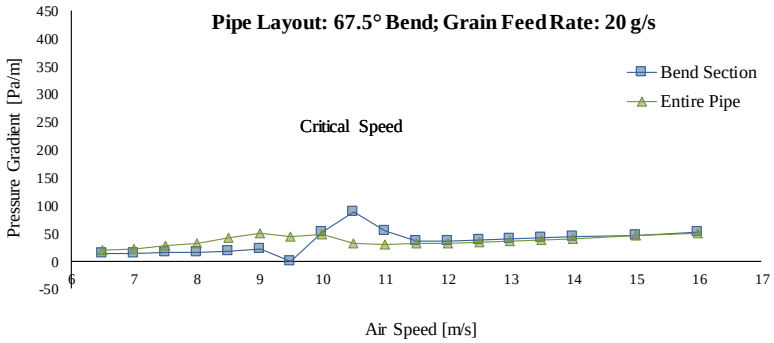

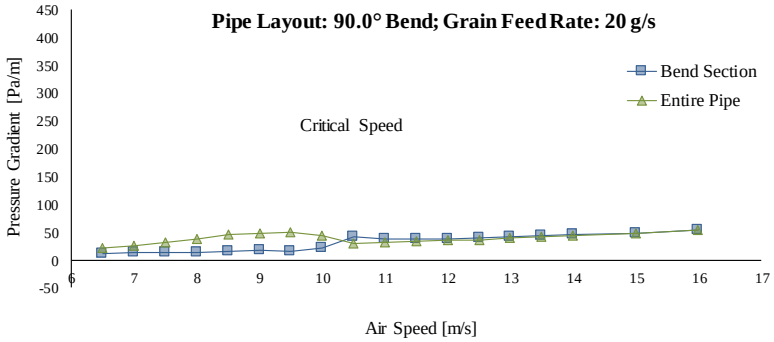

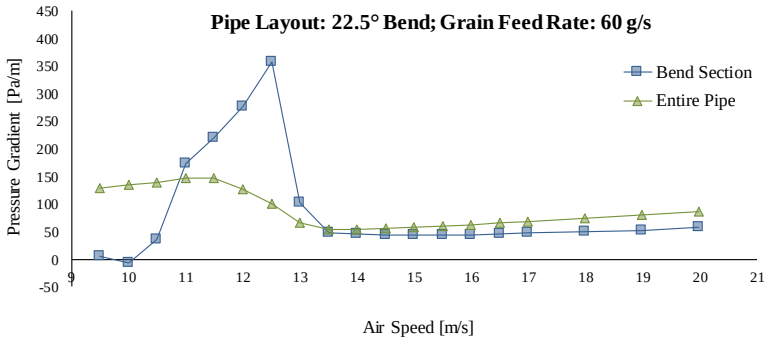
Pipe Layout: 22.5° Bend; Grain Feed Rate: 60 g/s
Pressure Gradient [Pa/m]
Air Speed [m/s]
Bend Section
Entire Pipe

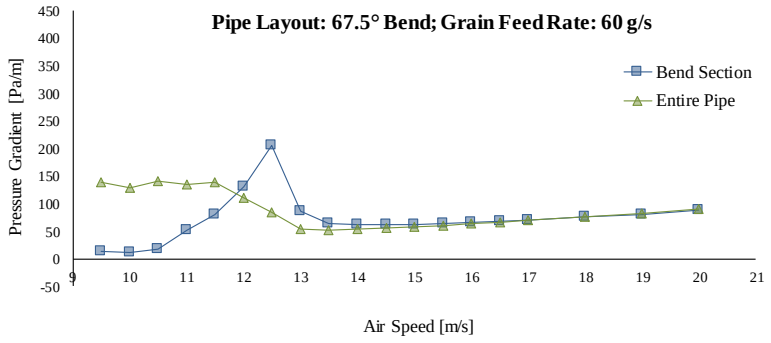
Pipe Layout: 67.5° Bend; Grain Feed Rate: 60 g/s
Pressure Gradient [Pa/m]
Air Speed [m/s]
Bend Section
Entire Pipe

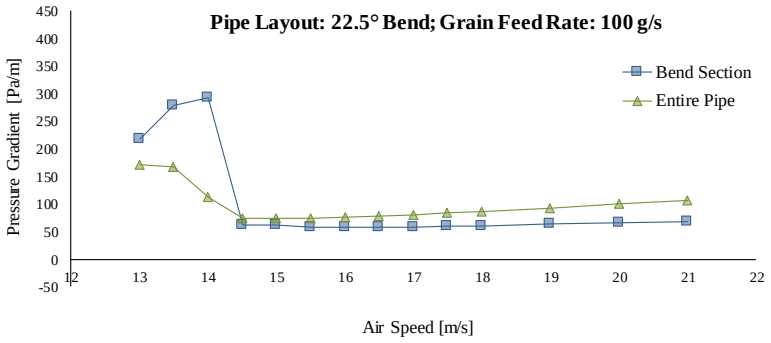
Pipe Layout: 22.5° Bend; Grain Feed Rate: 100 g/s
Pressure Gradient [Pa/m]
Air Speed [m/s]
Bend Section
Entire Pipe

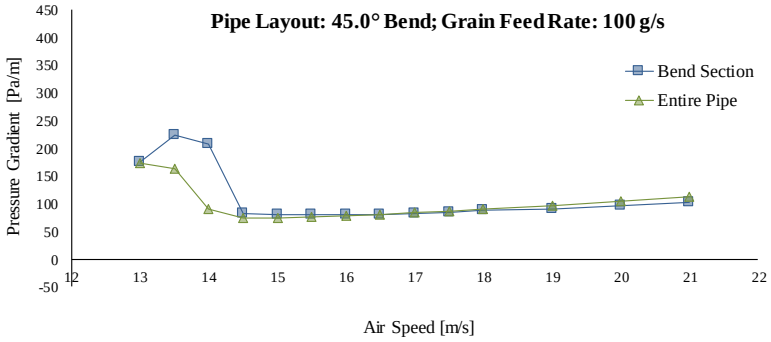
Pipe Layout: 45.0° Bend; Grain Feed Rate: 100 g/s
Pressure Gradient [Pa/m]
Air Speed [m/s]
Bend Section
Entire Pipe

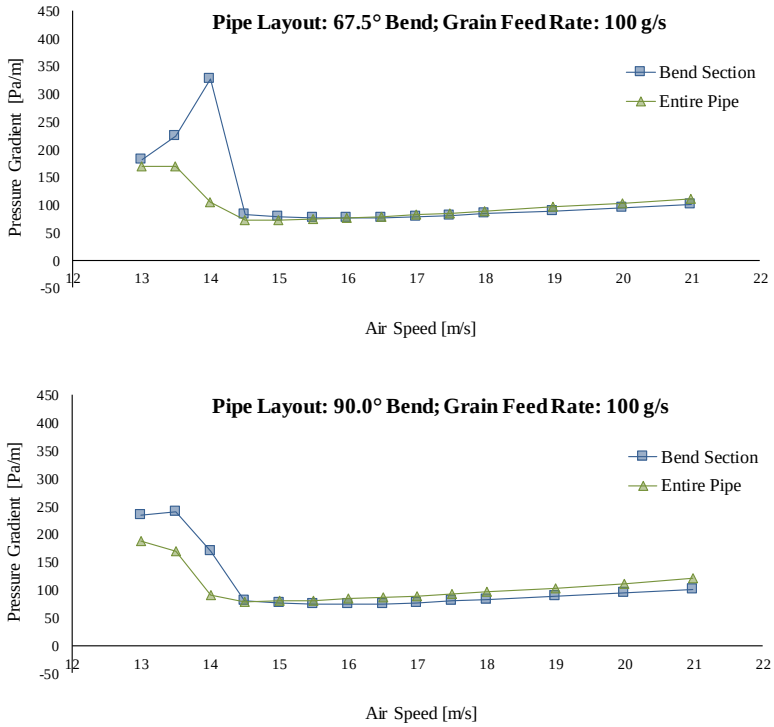

Figure B.3: Trend of local pressure gradient in bend section vs. average pressure gradient in entire pipe. Respective pipe layout and grain feed rate are given in the chart title.

Downstream of bend

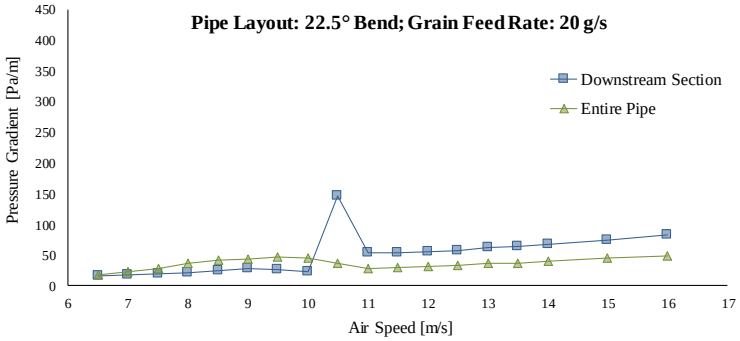

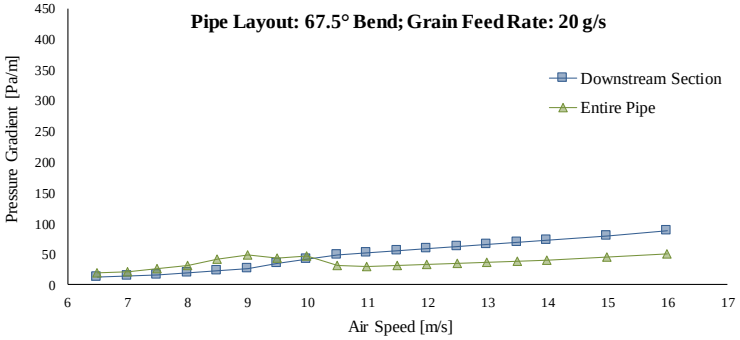

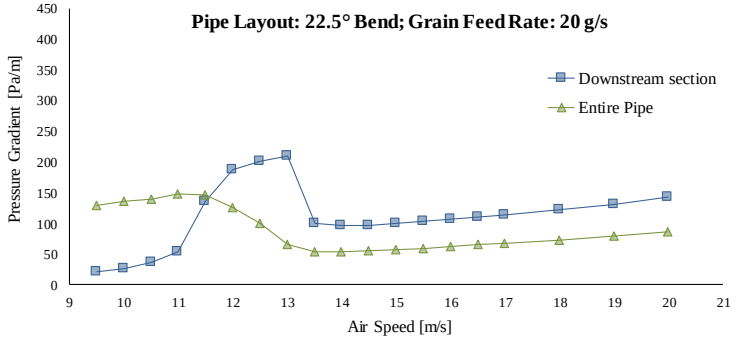

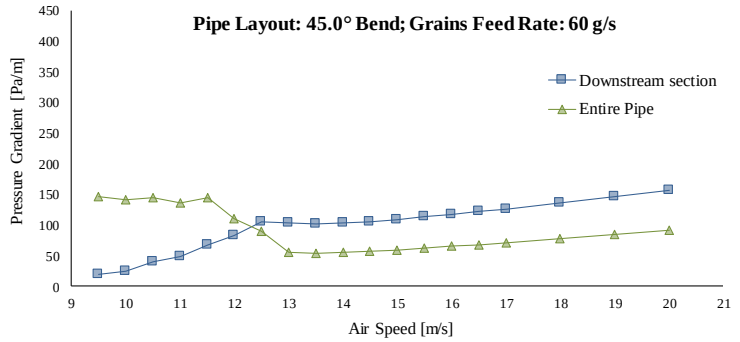

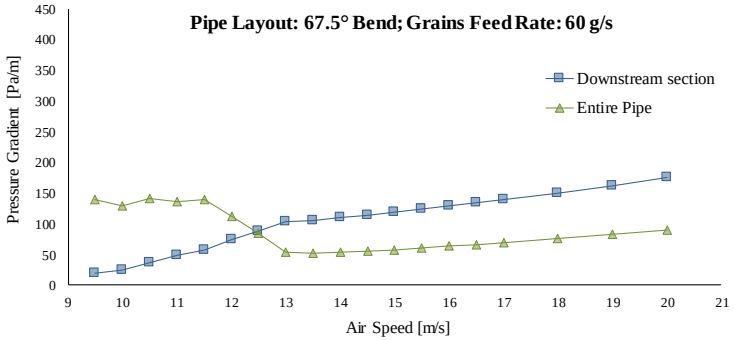

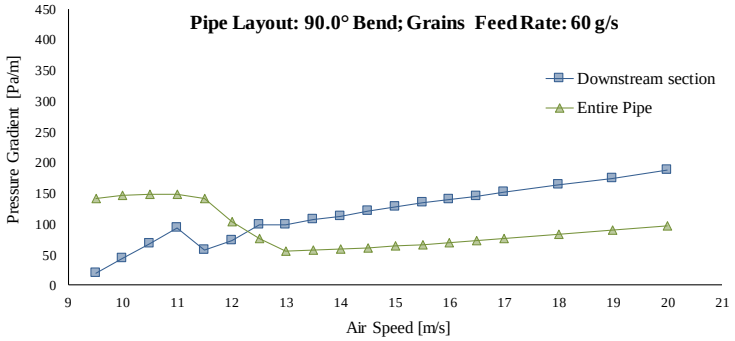

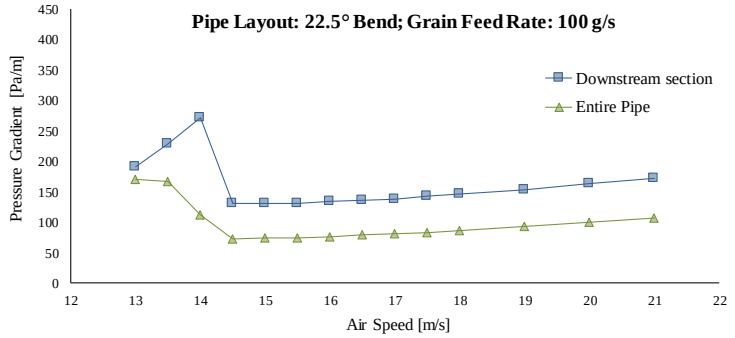

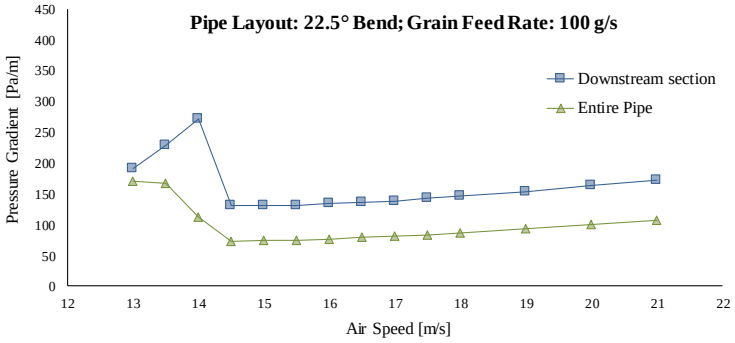

Figure B.4: Trend of local pressure gradient in downstream of bend section vs. average pressure gradient in entire pipe. Respective pipe layout and grain feed rate are given in the chart title.

Variation in pressure-gradient along the pipe

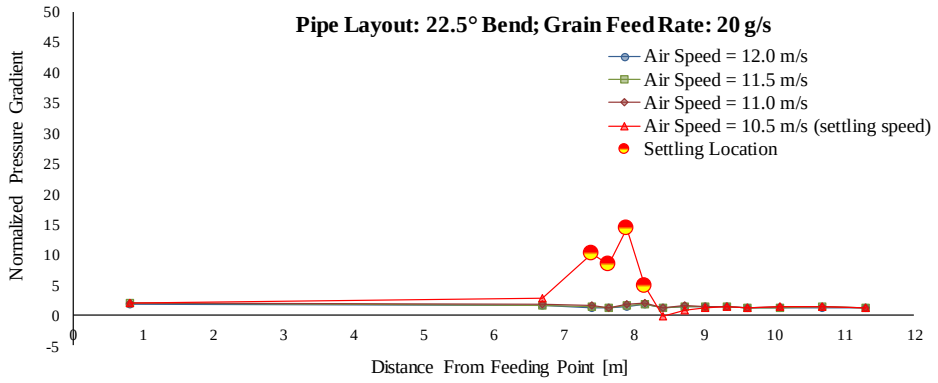

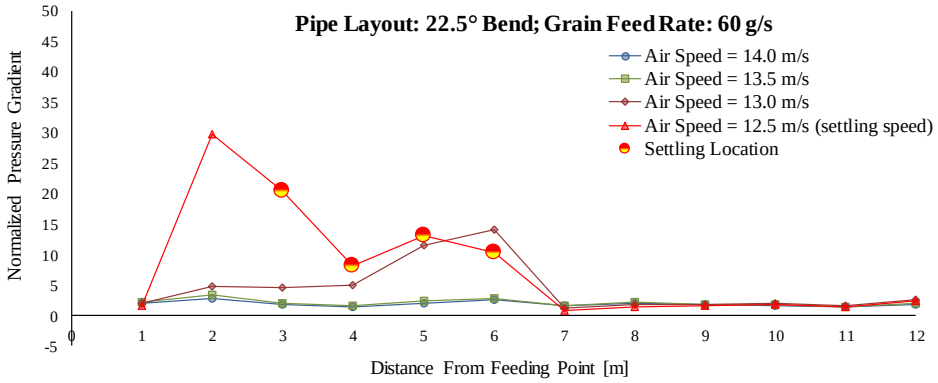

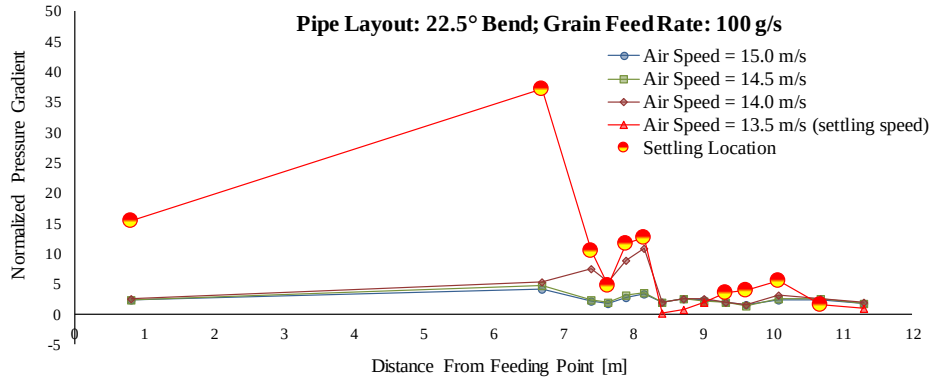

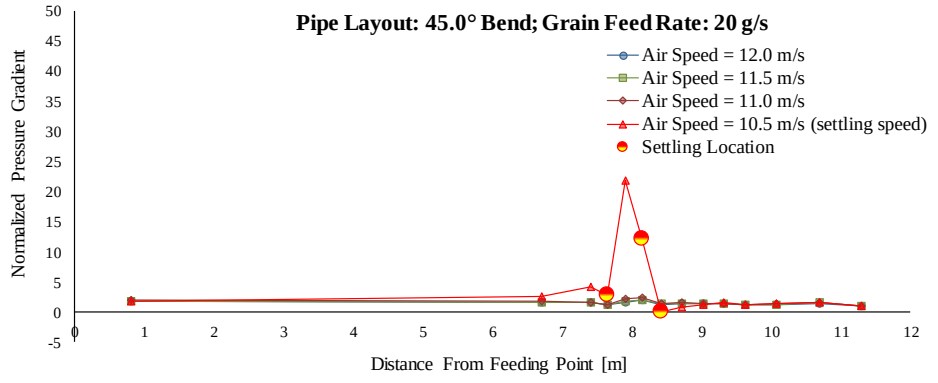

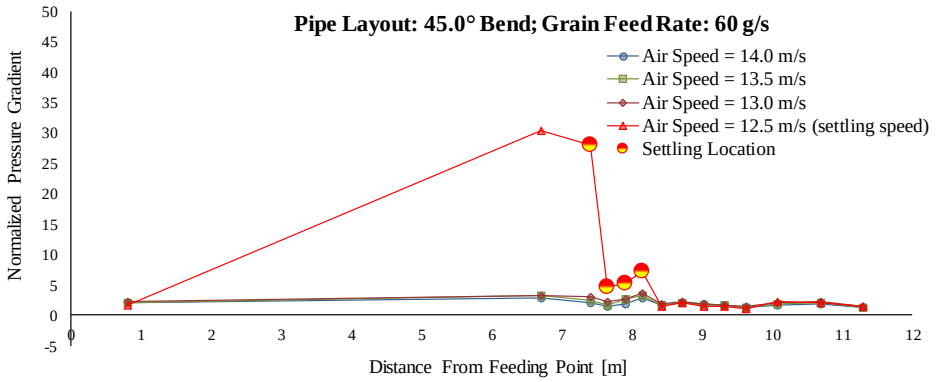
Pipe Layout: 45.0° Bend; Grain Feed Rate: 60 g/s
Air Speed = 14.0 m/s
Air Speed = 13.5 m/s
Air Speed = 13.0 m/s
Air Speed = 12.5 m/s (settling speed)
Settling Location
Normalized Pressure Gradient
Distance From Feeding Point [m]

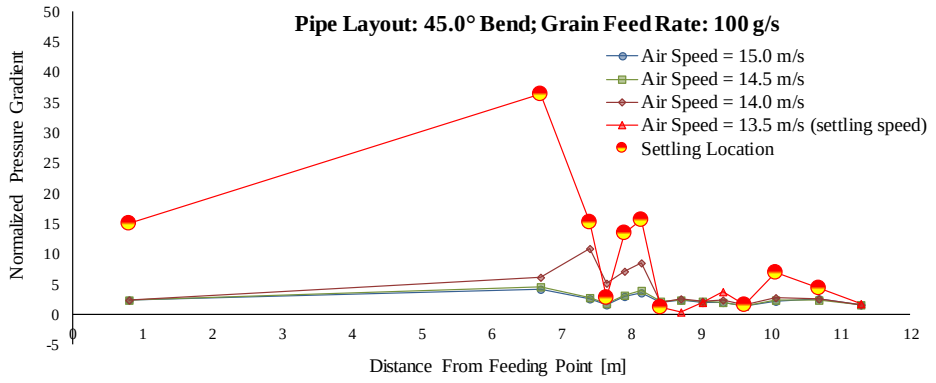
Pipe Layout: 45.0° Bend; Grain Feed Rate: 100 g/s
Air Speed = 15.0 m/s
Air Speed = 14.5 m/s
Air Speed = 14.0 m/s
Air Speed = 13.5 m/s (settling speed)
Settling Location
Normalized Pressure Gradient
Distance From Feeding Point [m]

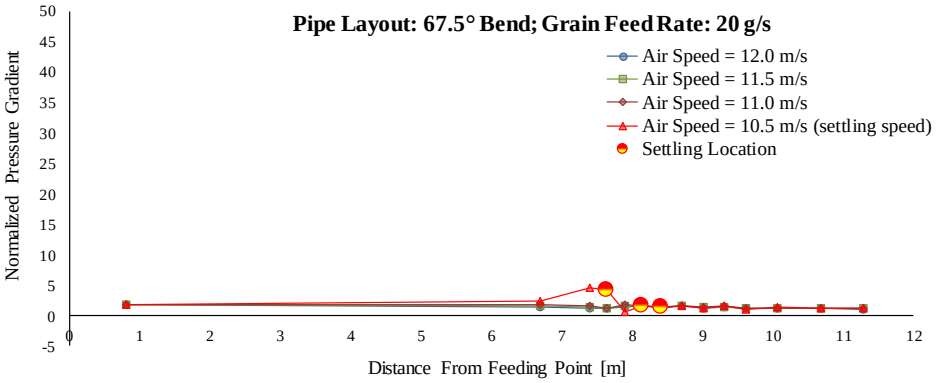
Pipe Layout: 67.5° Bend; Grain Feed Rate: 20 g/s
Air Speed = 12.0 m/s
Air Speed = 11.5 m/s
Air Speed = 11.0 m/s
Air Speed = 10.5 m/s (settling speed)
Settling Location
Normalized Pressure Gradient
Distance From Feeding Point [m]

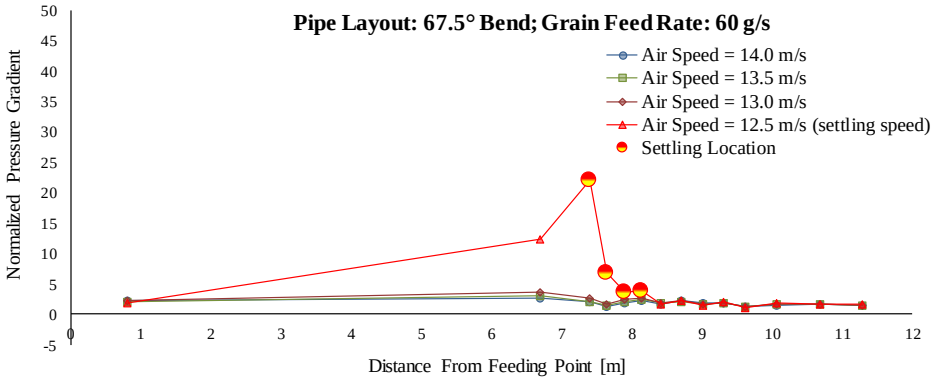
Pipe Layout: 67.5° Bend; Grain Feed Rate: 60 g/s
Air Speed = 14.0 m/s
Air Speed = 13.5 m/s
Air Speed = 13.0 m/s
Air Speed = 12.5 m/s (settling speed)
Settling Location
Normalized Pressure Gradient
Distance From Feeding Point [m]

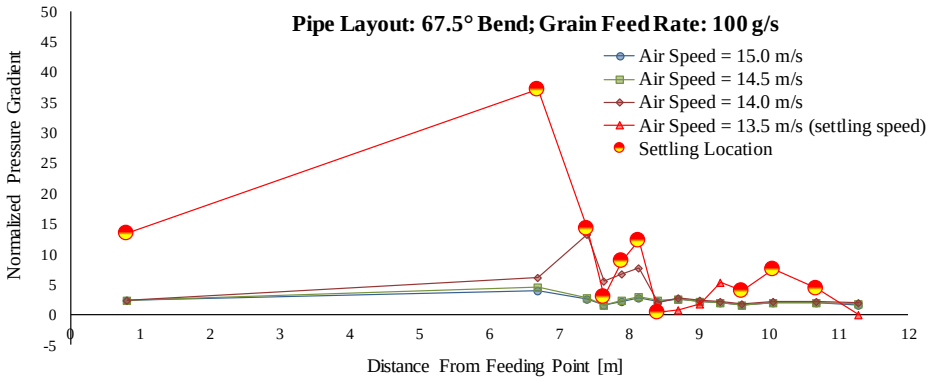

Figure B.5: Trend of normalized press gradient in various local sections along the pipe Respective pipe layout and grain feed rate are given in the chart title.